REPORT DOCUMENTATION PAGE

Form Approved OMB NO. 0704-0188

The public reporting burden for this collection of information is estimated to average 1 hour per response, including the time for reviewing instructions, searching existing data sources, gathering and maintaining the data needed, and completing and reviewing the collection of information. Send comments regarding this burden estimate or any other aspect of this collection of information, including suggesstions for reducing this burden, to Washington Headquarters Services, Directorate for Information Operations and Reports, 1215 Jefferson Davis Highway, Suite 1204, Arlington VA, 22202-4302. Respondents should be aware that notwithstanding any other provision of law, no person shall be subject to any oenalty for failing to comply with a collection of information if it does not display a currently valid OMB control number.
PLEASE DO NOT RETURN YOUR FORM TO THE ABOVE ADDRESS.

1. REPORT DATE (DD-MM-YYYY)	2. REPORT TYPE	3. DATES COVERED (From - To)
25-11-2015	Final Report	1-Sep-2009 - 31-Aug-2015

4. TITLE AND SUBTITLE
Final Report: Multifunctional Antenna Techniques

5a. CONTRACT NUMBER
W911NF-09-1-0429

5b. GRANT NUMBER

5c. PROGRAM ELEMENT NUMBER
611103

6. AUTHORS
Gregory H. Huff

5d. PROJECT NUMBER

5e. TASK NUMBER

5f. WORK UNIT NUMBER

7. PERFORMING ORGANIZATION NAMES AND ADDRESSES
Texas Engineering Experiment Station
SRS
400 Harvey Mitchell Parkway South, Suite 300
College Station, TX 77845 -4375

8. PERFORMING ORGANIZATION REPORT NUMBER

9. SPONSORING/MONITORING AGENCY NAME(S) AND ADDRESS (ES)
U.S. Army Research Office
P.O. Box 12211
Research Triangle Park, NC 27709-2211

10. SPONSOR/MONITOR'S ACRONYM(S)
ARO

11. SPONSOR/MONITOR'S REPORT NUMBER(S)
54724-EL-PCS.33

12. DISTRIBUTION AVAILIBILITY STATEMENT
Approved for Public Release; Distribution Unlimited

13. SUPPLEMENTARY NOTES
The views, opinions and/or findings contained in this report are those of the author(s) and should not contrued as an official Department of the Army position, policy or decision, unless so designated by other documentation.

14. ABSTRACT
This final report summarizes the activities and achievements of Grant #W911NF-09-1-0429 (“PECASE: Multifunctional Antenna Techniques”). Significant progress was made in all aspects of the proposed research program. This includes theory, design, and experiments on Aperchassis (structural antenna concepts), Antensors (sensor-antenna hybrids), and dynamic networks (constellations of multifunctional platforms).

15. SUBJECT TERMS
Multifunctional antennas, reconfigurable antennas, electromagnetics

16. SECURITY CLASSIFICATION OF:			17. LIMITATION OF ABSTRACT	15. NUMBER OF PAGES	19a. NAME OF RESPONSIBLE PERSON
a. REPORT	b. ABSTRACT	c. THIS PAGE			Gregory Huff
UU	UU	UU	UU		19b. TELEPHONE NUMBER 979-862-4161

Report Title

Final Report: Multifunctional Antenna Techniques

ABSTRACT

This final report summarizes the activities and achievements of Grant #W911NF-09-1-0429 ("PECASE: Multifunctional Antenna Techniques"). Significant progress was made in all aspects of the proposed research program. This includes theory, design, and experiments on Aperchassis (structural antenna concepts), Antensors (sensor-antenna hybrids), and dynamic networks (constellations of multifunctional platforms).

Enter List of papers submitted or published that acknowledge ARO support from the start of the project to the date of this printing. List the papers, including journal references, in the following categories:

(a) Papers published in peer-reviewed journals (N/A for none)

Received	Paper
08/29/2013 16.00	Jeffrey Jensen, Gregory Huff, Jean-Francois Chamberland-Tremblay. Cognitive Motion-Dynamic Tethering of a Phased Array to an Android Smartphone, IEEE Transactions on Antennas and Propagation, (06 2013): 0. doi: 10.1109/TAP.2013.2267201
08/29/2013 18.00	Gregory H. Huff, David L. Rolando. A Geometrically-Appropriate Cavity Model for a Spherical Inverted-F Antenna (SIFA), IEEE Transactions on Antennas and Propagation, (05 2013): 2404. doi: 10.1109/TAP.2013.2246533
08/29/2013 22.00	Teng-Kai Chen, Gregory H. Huff. Modal Resistance of Spiral Antenna, Journal of Electromagnetic Analysis and Applications, (06 2013): 223. doi: 10.4236/jemaa.2013.55036
08/29/2014 26.00	Teng-Kai Chen, Gregory H. Huff. Transmission line analysis of the Archimedean spiral antenna in free space, Journal of Electromagnetic Waves and Applications, (04 2014): 1175. doi: 10.1080/09205071.2014.909295
08/29/2014 27.00	TengKai Chen, Gregory Huff. Travelling Wave Mechanism and Novel Analysis of the Planar Archimedean Spiral Antenna in Free Space, Progress In Electromagnetics Research C, (04 2014): 287. doi:
08/29/2014 24.00	Kristopher Buchanan, Gregory Huff. A Stochastic Mathematical Framework for the Analysis of Spherically-Bound Random Arrays, IEEE Transactions on Antennas and Propagation, (06 2014): 3002. doi: 10.1109/TAP.2014.2313142
08/29/2014 23.00	TengKai Chen, Gregory Huff. On the Constant Input Impedance of the Archimedean Spiral Antenna in Free-Space, IEEE Transactions on Antennas and Propagation, (07 2014): 3869. doi: 10.1109/TAP.2014.2320760
08/31/2011 1.00	Teng-Kai Chen, Gregory H. Huff. Stripline-Fed Archimedean Spiral Antenna, IEEE Antennas and Wireless Propagation Letters, (04 2011): 346. doi: 10.1109/LAWP.2011.2141971
TOTAL:	**8**

Number of Papers published in peer-reviewed journals:

(b) Papers published in non-peer-reviewed journals (N/A for none)

Received	Paper

TOTAL:

Number of Papers published in non peer-reviewed journals:

(c) Presentations

Number of Presentations: 0.00

Non Peer-Reviewed Conference Proceeding publications (other than abstracts):

Received	Paper
08/28/2012	14.00 Gregory H. Huff, Teng-Kai Chen, Kristopher Buchanan, Joel D. Barrera, Frank Drummond, Amanda Couch, Nick Brennan, Christopher Kirkland, Quinn Manley. DEVELOPMENT OF A DISC-SHAPED UAV BASED ON THE ARCHIMEDEANSPIRAL ANTENNA, Antenna Applications Symposium. 23-SEP-11, . : ,

TOTAL: **1**

Number of Non Peer-Reviewed Conference Proceeding publications (other than abstracts):

Peer-Reviewed Conference Proceeding publications (other than abstracts):

Received	Paper
08/28/2012 6.00	Jean-Francois Chamberland, Henry Pfister, Raktim Bhattacharya, Zhenchun Xia, Gregory H. Huff. Direction of arrival estimation using canonical and crystallographic volumetric element configurations, 2012 6th European Conference on Antennas and Propagation (EuCAP). 25-MAR-12, Prague, Czech Republic. : ,
08/28/2012 7.00	Santhosh Kumar, Jean-Francois Chamberland, Pankaj Parag, Gregory H. Huff. Detecting the presence of a proximate cellular user through distributed femtocell sensing, 2012 IEEE 7th Sensor Array and Multichannel Signal Processing Workshop (SAM). 16-JUN-12, Hoboken, NJ, USA. : ,
08/29/2013 21.00	Teng-Kai Chen, Gregory H. Huff. DEVELOPMENT AND ANALYSIS OF A STRIPLINE ARCHIMEDEAN SNAIL ANTENNA FOR DISC-SHAPED UNMANNED AERIAL VEHICLE APPLICATIONS, Progress In Electromagnetics Research Symposium -Taipei. 25-MAR-13, . : ,
08/29/2013 19.00	Teng-Kai Chen, Gregory H. Huff. Investigation on the Input Impedance of Two-Arm Frequency-Independent Antennas in Free Space, 2013 IEEE AP-S/USNC-URSI Symposium. 11-JUL-13, . : ,
08/29/2014 28.00	David Rolando, Gregory Huff. Frequency Selective Surface Design using a Lattice Based Equivallent Circuit Model, Allerton Antenna Applications Symposium. 18-SEP-13, . : ,
08/29/2014 29.00	Russel Haley, Quinn Manley, Robert Moore, Zhenchun Xia, Joel Barrera, Gregory Huff, Jean Chamberland, Elijas Foster. A direction of arrival system using polarization reconfigurable antennas, smartphones, and cloud based processing, Allerton Antenna Applications Symposium. 18-SEP-13, . : ,
08/29/2014 30.00	Elijas Foster, Russell Haley, Quinn Manley, Robert Moore, Zhenchun Xia, Joel Barrera, Gregory Huff, JeanFrancois Chamberland. A direction of arrival system using polarization reconfigurable antennas, smartphones, and cloud based processing, Allerton Antenna Applications Symposium. 18-SEP-13, . : ,
09/12/2011 5.00	Kristopher Buchanan, Gregory H. Huff. A Comparison of Geometrically Bound Random Arrays in Euclidean Space, 2011 IEEE AP-S/URSI Intl. Symp. on Antennas and Propagation. 06-JUL-11, . : ,
11/25/2015 32.00	Jeffrey S. Jensen, Gregory H. Huff. A COMPUTER VISION ASSISTED FRAMEWORK FOR BEAMFORMING OF RANDOM VOLUMETRIC ARRAYS , Antenna Application Symposium. 22-SEP-15, . : ,
TOTAL:	**9**

Number of Peer-Reviewed Conference Proceeding publications (other than abstracts):

(d) Manuscripts

Received		Paper
08/28/2012	9.00	Teng-Kai Chen, Gregory H. Huff. On the Input Impedance of Two-Arm Gap-Fed Complementary Archimedean Spiral Antennas on Dielectric Substrates, IEEE Transactions on Propagation and Antennas (08 2011)
08/28/2012	13.00	Teng-Kai Chen, Gregory H. Huff. Analytic Analysis of MultilayeredPeriodic Coplanar Waveguides, IEEE MTT Transactions (06 2012)
08/28/2012	12.00	David L. Rolando, Gregory H. Huff. A Geometrically-Appropriate Cavity Model for a Spherical Inverted-F Antenna (SIFA), IEEE Antennas and Propagaton Transactions (05 2012)
08/28/2012	11.00	Kristopher Buchanan, Gregory H. Huff. Analysis of Spherically Bound Random Arrays, IEEE Antennas and Propagaton Transactions (05 2012)
08/28/2012	10.00	Teng-Kai Chen, Gregory H. Huff. A Note to the Input Impedance of Two-Arm Frequency-Independent Antennas in Free Space, IEEE Transactions on Propagation and Antennas (04 2012)
08/29/2013	17.00	Gregory H. Huff, Teng-Kai Chen. Analytical Investigation of Periodic Coplanar Waveguides, Progress In Electromagnetics Research C (05 2013)
TOTAL:		**6**

Number of Manuscripts:

Books

Received		Book
TOTAL:		

Received	Book Chapter

TOTAL:

Patents Submitted

Patents Awarded

Awards

Graduate Students

NAME	PERCENT_SUPPORTED	Discipline
Jeffrey S. Jensen	1.00	
Frank Drummond	0.25	
Taahir Ahmed	0.13	
David Grayson	0.50	
FTE Equivalent:	**1.88**	
Total Number:	**4**	

Names of Post Doctorates

NAME	PERCENT_SUPPORTED
FTE Equivalent:	
Total Number:	

Names of Faculty Supported

NAME	PERCENT_SUPPORTED	National Academy Member
Gregory H. Huff	0.08	
FTE Equivalent:	**0.08**	
Total Number:	**1**	

Names of Under Graduate students supported

NAME	PERCENT_SUPPORTED	Discipline
Lisa Smith	0.25	Electrical Engineering
Deanna Sessions	0.25	Electrical Engineering
FTE Equivalent:	**0.50**	
Total Number:	**2**	

Student Metrics

This section only applies to graduating undergraduates supported by this agreement in this reporting period

The number of undergraduates funded by this agreement who graduated during this period: 2.00

The number of undergraduates funded by this agreement who graduated during this period with a degree in science, mathematics, engineering, or technology fields:..... 2.00

The number of undergraduates funded by your agreement who graduated during this period and will continue to pursue a graduate or Ph.D. degree in science, mathematics, engineering, or technology fields:..... 2.00

Number of graduating undergraduates who achieved a 3.5 GPA to 4.0 (4.0 max scale):..... 2.00

Number of graduating undergraduates funded by a DoD funded Center of Excellence grant for Education, Research and Engineering:..... 0.00

The number of undergraduates funded by your agreement who graduated during this period and intend to work for the Department of Defense 1.00

The number of undergraduates funded by your agreement who graduated during this period and will receive scholarships or fellowships for further studies in science, mathematics, engineering or technology fields:..... 2.00

Names of Personnel receiving masters degrees

NAME
Total Number:

Names of personnel receiving PHDs

NAME
Jeffrey S. Jensen
Total Number: 1

Names of other research staff

NAME	PERCENT_SUPPORTED
FTE Equivalent:	
Total Number:	

Sub Contractors (DD882)

Inventions (DD882)

Scientific Progress

"See Attachment"

Technology Transfer

Report Type:	Final Progress Report
Proposal Number:	54724-EL-PCS
Grant Number:	W911NF-09-1-0429
Proposal Title:	PECASE: Multifunctional Antenna Techniques
Principle Investigator:	Gregory H. Huff
Institution:	Texas A&M University
Performance Period:	01-SEP-2009 to 31-AUG-2015

Abstract

This final report summarizes the activities and achievements of Grant #W911NF-09-1-0429 ("PECASE: Multifunctional Antenna Techniques"). Significant progress was made in all aspects of the proposed research program. This includes theory, design, and experiments on Aperchassis (structural antenna concepts), Antensors (sensor-antenna hybrids), and dynamic networks (constellations of multifunctional platforms).

Scientific Progress

The scientific progress presented in this final report for Grant #W911NF-09-1-0429 ("PECASE: Multifunctional Antenna Techniques") occurred during the performance period beginning 01-SEP-2009 and ending 31-AUG-2015. This includes the original five year performance period of the PECASE (beginning 01-SEP-2009) and a one year no-cost extension (beginning 01-SEP-2014). This report provides a detailed summary of the experimental, analytical, numerical, and educational activities supported by this project, and includes details on the educational and professional/workforce training that was also made possible through this project. Significant progress was achieved and the results from research and educational activities have been disseminated in numerous conference and symposium talks, and a number of manuscripts are in various stages of preparation and review in peer-reviewed journals (in addition to those published during the active status of this project). The major scientific and engineering accomplishments facilitated by this project's support are provided in the following subsections; these are delineated by research thrusts and their respective proposed goals and achievements.

Thrust 1: Aperchassis – Examine the functional balance between bandwidth, size, and weight limitations in HF, VHF, and UHF structurally-functionalized apertures for multifunction platforms

Research Goal 1.1 Aperchassis: Develop design methodologies for internally-fed spirals, tapered-slots, and bow-tie antennas with functionalizable (internal) volumes and instantaneous operation from 2 MHz to 2 GHz

Achievement 1.1.a *An extensible design methodology for electrically large conformal antennas*
PI: Gregory H. Huff
PhD Graduate Student: Teng-Kai Chen
Undergraduate Student: Amanda M. Couch

A design methodology for electrically large conformal antennas was conceived and demonstrated experimentally. This method is applicable to many planar gap-fed traveling-wave antennas (spirals, bowties, etc.), and the antenna is viewed as multifunctional structural platform that can also serve as a broadband feed network, balun, and radiator. The design process for the antenna begins by inspecting the topology and electromagnetic operation for the electrically large planar antenna (or family of antennas); this is to evaluate the real estate on the planar structure that can be sufficiently isolated from the radiation mechanism of the antenna and transformed into a TEM transmission line feed network. Antenna topologies with an even number of excitation terminals (two and four-arm spirals, two and for arm bowties, etc.) have been examined in this project since differential and/or quadrature excitation is commonly used to excite their radiating modes. These subsets of antennas also have rotational symmetry, such that the even- or odd-numbered subset of 'arms' of the radiating structure can be chosen to transform into a stripline feed manifold.

The process of transforming the selected antenna arm(s) into a feed structure begins by tailoring the slot-to-metal ratio of the canonical gap-fed (terminal-driven) antenna structure for the desired feed line and/or system impedance. Once this has been completed, the planar antenna is embedded into the center of a two-layer substrate configuration that makes it possible to achieve three layers of metallization (a top ground, middle signal layer, and bottom ground). The arm(s) selected for transformation to a feed structure are then duplicated and translated vertically to reside on the top and bottom ground layers. A signal trace is then routed between these two metal layers to create a stripline feed network that extends through the original gap and connects to the remaining arm(s) that reside in the middle signal metallization layer. Once this has been accomplished, the antenna becomes an

inward-fed radiating structure. The transition across the gap that was present in the original planar topology resembles the Dyson balun developed to excite planar and conical log periodic spiral antennas; the major accomplishment in this work is the transformation of this concept into a design methodology that shields the feed network and enables the development of additional functionality beyond the excitation of the antenna.

Fig. 1 shows the result of this process for an Archimedean spiral antenna, which is one of the antenna topologies that have been studied extensively using this design mythology (radial dipoles and bowties have also been examined). The top diagram shows the cross-section of the antenna after this transformation, and the bottom diagrams show the multilayer stripline topology that conforms to the spiral's winding and expansion parameters. The signal trace that is extruded through spiral's center, where the gap feed is located and connected to the second (unmodified) spiral arm, also resides on the signal layer. The upper and lower ground layers form the second arm of the spiral since they each maintain the same electromagnetic potential (with respect to the center conductor and first arm of the spiral). This provides a structurally integrated feed network which shares it role as both the antenna structure and as the ground for the transmission line feed network. This particular transformation is for a spiral designed to maintain its 90 [illegible] but the tapered line and [illegible] from 2 GHz to 18 GHz integrated impedance transformer (discussed later in this Thrust) illustrates the capability to functionalize an antenna platform. The formalized design process has been a key development in accelerating the development of more advanced and compact radiating systems.

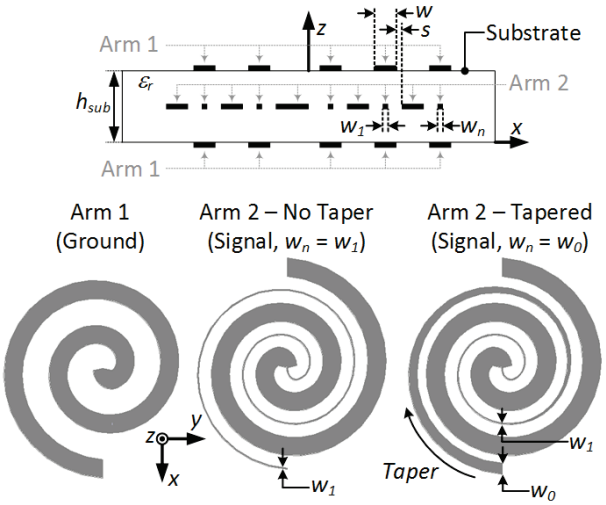

Fig. 1 Stripline-fed spiral antenna: (top) cross-section of the stripline-fed topology, (bottom-left) stripline grounds formed by Arm 1 at z = 0 and h_{sub}; (bottom-center) stripline signal line (Arm 2) at z = 0.5 h_{sub} with no taper and $w_n = w_1$; and (bottom-right) stripline signal line (Arm 2) at z = 0.5 h_{sub} with curvilinear taper between w_0 and w_1.

Achievement 1.1.b A periodic coplanar waveguide (PCPW) transmission line model for the input impedance of multi-arm Archimedean spiral antennas
PI: Gregory H. Huff
PhD Graduate Student: Teng-Kai Chen

An analytical model has been developed to predict the input impedance of multi-arm Archimedean spiral antennas. This model examines the relationship between metal width and arm spacing of a planar printed spiral antenna and uses this to examine the input impedance and radiating mechanism. Observations from an empirical investigation using finite element simulations were used first to decompose the spiral into an equivalent transmission line structure, and isolate the physical

mechanisms responsible for impedance and radiation behavior. Fig. 2 provides an illustration of this process for a nominal design of the Archimedean spiral antenna shown on the left side of (including the expanded view of the gap-fed central section). The diagram on the middle-right side of this figure shows the insertion of two perfect magnetic conducting (PMC) boundaries that are used to create a closed surface and define an equivalent slotline transmission line. In this figure, Port 1 refers to the gap feed (excitation) of the spiral and Ports 2 and 3 refer to the traveling wave mode of the spiral. This model provides an empirical description of both propagation and radiation and it is complementary to concepts provided by band theory, which predicts the radiating regions of the antenna based on resonant circumferences of rings inscribed by the spiral. This decomposition of the antenna also provides the starting point for the analytical model of the input impedance of the Archimedean spiral.

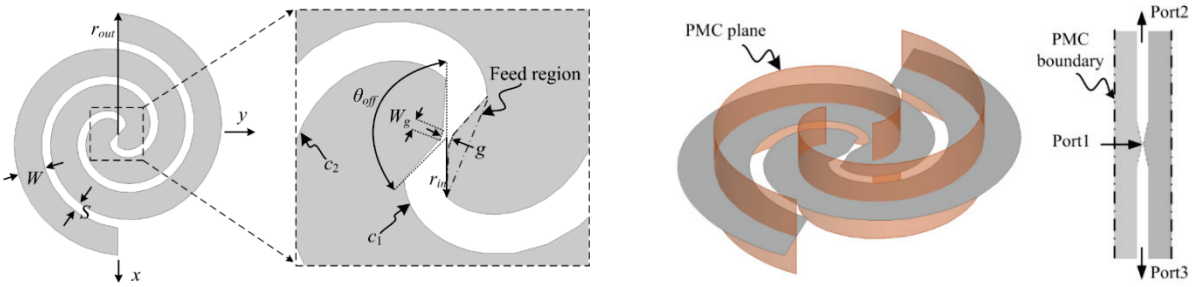

Fig. 2 Layout (left) and expanded view of the feed section (middle-left) of the two-arm gap-fed Archimedean spiral antenna in free space with non-negligible metal width, insertion PMC boundaries to isolate the radiation and propagation on the spiral (middle-right), and equivalent transmission line structure of the spiral (right) .

The diagram on the left side of Fig. 3 illustrates the cross-section of the transmission line shown on the right side of Fig. 2. Conformal mapping techniques were used to decompose this physical model further and enable the use of conformal mapping techniques to calculate the input impedance of the transmission line created by the spiral geometry. The symmetric field distribution of the PCPW facilitates the placement of the PEC and PMC boundaries shown on the left diagram in Fig. 3. This can be represented by the equivalent circuit shown on the right side of Fig. 3 . The total capacitance C_a for one periodic section of PCPW can then be evaluated using this model. The z-plane for this topology shown in Fig. 5(b) has the coordinates z_b = W/2 + S/2, z_c = W/2 and z_d = 0. These are mapped to the t-plane and then w-plane using conformal mapping techniques. Once this capacitance is obtained, a closed-form expression for the input impedance of the spiral can be obtained. This is under the assumption that the spiral is a leaky wave structure, with an attenuation coefficient that creates a minimal disturbance of this impedance, such that if all energy is radiated the spiral will appear as an infinitely long line with the characteristic impedance calculated by the method described here.

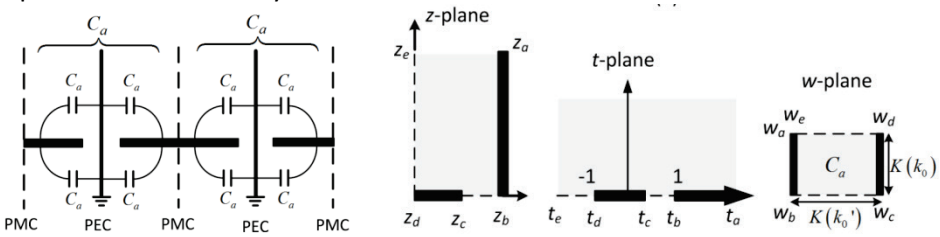

Fig. 3 Calculation of P.U.L. capacitance C_a of slotline with lateral PMC in free space: (left) schematic electric field distribution with virtual plane and (right) conformal mapping steps from z-plane onto t-plane and then onto w-plane.

Fig. 4 shows the characteristic impedance of PCPW operating in the common slot-line mode in free space as a function of the metallization ratio χ. A very wide range of arm width *W* and spacings *S* are accounted for in this plot ($0.05 \le \chi \le 0.95$), and the results shown are analyzed at 10 GHz in full-wave

simulations. The results obtained by conformal mapping remains in very good agreement with simulations when no higher order slot-line modes exist. This model provides a new method for analyzing these antennas, and a comparison to the most widely accepted coplanar-strips model has been added to Fig. 4 to illustrate the accuracy provided by this model.

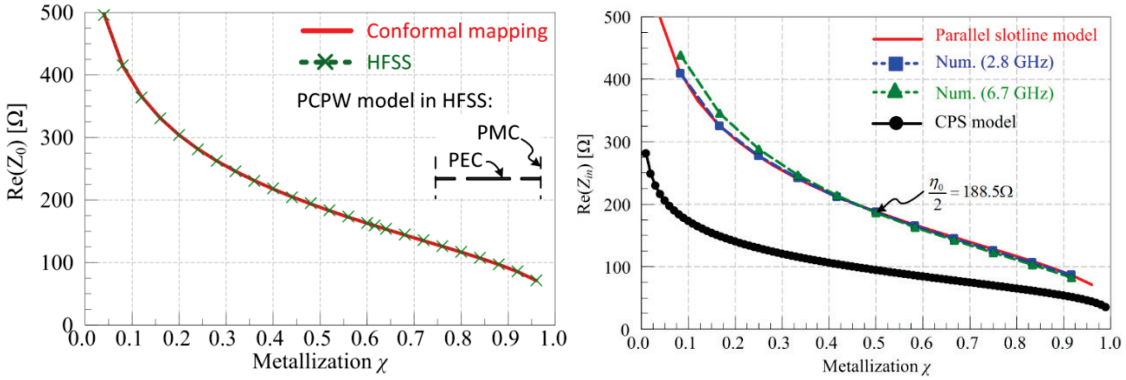

Fig. 4 (Left) Real-valued characteristic impedance as a function of metallization ratio obtained using conformal mapping and numerical simulation as PCPW operating in the common slot-line mode in free space, and (right) the analytical (parallel slotline model, a.k.a. CPCW) and simulated (finite-element) input impedance of Archimedean spiral antennas in free space, compared with the coplanar strips (CPS) model proposed in earlier models.

Achievement 1.1.c A fundamental reevaluation of complementary antenna topologies
PI: Gregory H. Huff
PhD Graduate Student: Teng-Kai Chen

The novel analysis of the radiation mechanism and input impedance using conformal mapping techniques provided a closed-form function requiring only the metallization ratio to evaluate the input impedance. Given the often-described self-complementary nature of spirals and other antennas, this model provided new insight into the fundamental discussion on the complementary impedance of these structures. Full-wave numerical simulations, Babinet's principle, and fabricated antennas were pursued in this project to demonstrate the accuracy of proposed model and create a discussion on several misconceptions held about these antennas. The analytical model proposed in the previous section can be used to predict the input impedance for a variety of non-self-complementary spiral structures. Examination and discussion on the radiation mechanism and effects of other parameters such as feed taper were also investigated in a process similar to that described for the Archimedean spiral, and the input resistance of spiral antenna in free space can be predicted by the characteristic impedance of PCPW propagating Fig. 5 and Fig. 6 show three of the candidate antenna topologies examined, and a comparison of their input impedance as a function of metallization □.

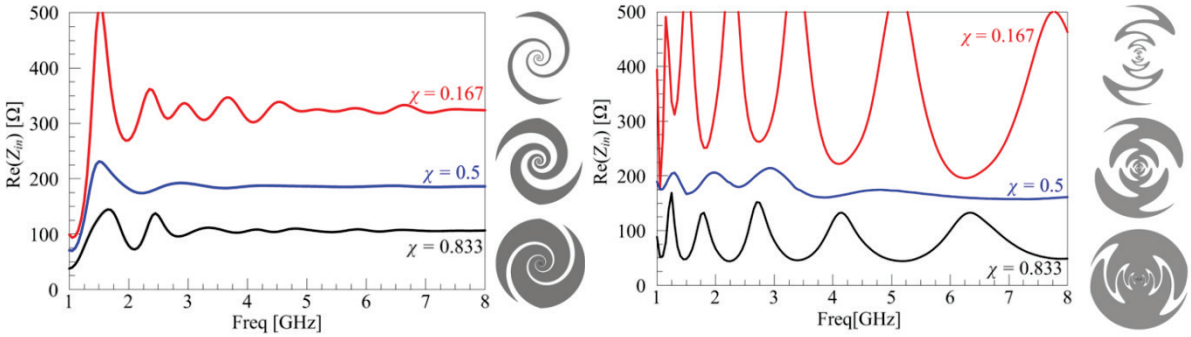

Fig. 5 (Left) Simulated real-valued input impedance of two-arm equiangular spiral antenna in free space and (Right) Simulated real-valued input impedance of two-arm sinuous antenna in free space.

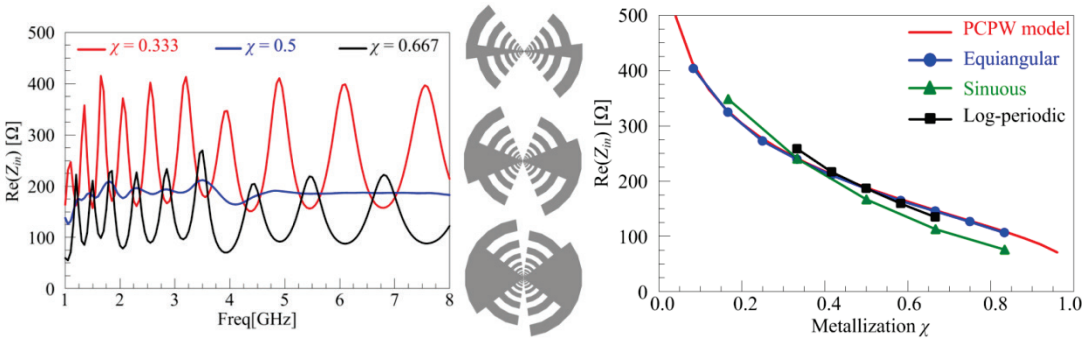

Fig. 6 (Left) Simulated real-valued input impedance of two-arm log-periodic antenna in free space and (Right)

All of these antennas are formed from geometrically complementary structures; the blue curve in each of these three impedance plots represents the self-complementary version of these antennas. Fig. 6 includes a comparison of the three simulated antennas along with the results obtained from the conformal mapping model using the periodic coplanar waveguide (PCPW) transmission line field structure. Several interesting conclusions can be drawn from the four plots in Fig. 5 and Fig. 6. First, the accuracy of the model is very dependent on the radiating mechanism, of which the Equiangular is most similar and the sinuous is most different than many external models propose. This is appropriate and expected behavior, but examining these structures in closer detail with these impedance curves raises a number of fundamental questions related to the actual physical operation of these classical antenna topologies which revolve around the physical radiating mechanism.

Beyond this, the overarching analysis of these antennas provides a somewhat intuitive, but important observation that can be made by examining the metallization ratio and considering the amount of shielded/grounded area that can be used to place components and other structures both into and onto the antenna (control surfaces, propulsion, etc.). Namely, these regions have locations that can support physical alterations that will not disrupt the performance-governing fields. The grey-hatched areas shown next to each impedance plots in Fig. 5 and Fig. 6 illustrate this, and support a conjectures that: first, slot-based structure will experience less physical interference from structural modifications (within reason); and second, the range of application-based options range from a linear (as in the log-periodic) to curvilinear (as in the spiral) centralized primary metallic surface from which components or control surfaces can be placed. Fig. 7 shows two of the fabricated planar log-periodic antennas with different metallization ratios being used to gather experimental observations; a more precise calibration procedure using time-domain gating could be used to remove the physical inconsistencies of the commercially-available coaxial cables being used, but the results obtained suggest they behave according to the analytical model and simulated structures.

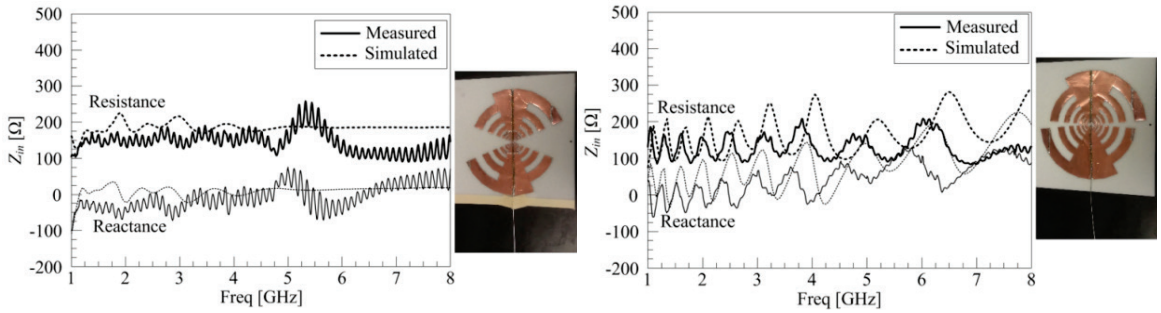

Fig. 7 Comparison of measured and simulated input impedance for a (Left) self-complementary log-periodic antenna design (right) non-self-complementary log-periodic antenna.

Research Goal 1.2 Provide internalized transmit and receive (T/R) functionality with distributed EM components (filters, impedance transformers, and baluns) in the antenna's volume

Achievement 1.2.a *Integration of baluns and filters into an inward-fed stripline-based spiral antenna*
PI: Gregory H. Huff
PhD Graduate Student: Teng-Kai Chen

The integration of a tapered stripline impedance transformer and a coupled-line stripline filter has been successfully integrated into the feed structure of broadband antennas. The tapered impedance transformer shown on the bottom-right side of Fig. 1 illustrates how complex electromagnetic structures can be integrated into curvilinear antenna topologies using the stripline transformation of the gap-fed antenna topology. The left diagram in Fig. 8 shows the final arrangement of the antenna in Fig. 1; this includes the inward-directed tapered broadband stripline impedance transformer that winds along one turn and remains centered and conformal to the spiral. The tapered impedance transformer makes measurements possible with a standard SMA probe feed, and this structure was designed and fabricated along with a tapered probe launch from a finite-ground microstrip line into the stepped-width transition (including two flanking vias) between microstrip and stripline topology of the spiral. The middle diagram in Fig. 8 shows the CAD model of the antenna and feed system. The left side of this figure provides the VSWR for the fabricated and simulated antenna (shown with and without probe-launch). The fabricated antenna does not show all layers as well as the CAD model so it has been left out of the diagrams; however, it was formed by mechanically milling both sides of two 20 mil Duroid 5880 substrates (the side of one sheet was etched completely). Nylon screws were used to mechanically fasten the two substrates together, but a nominally thin coating of PDMS was required to adhere the substrates tightly together (pressed together and thermally cured). The "Measurement (PDMS)" in the VSWR shown in Fig. 8 corresponds to this bonded structure.

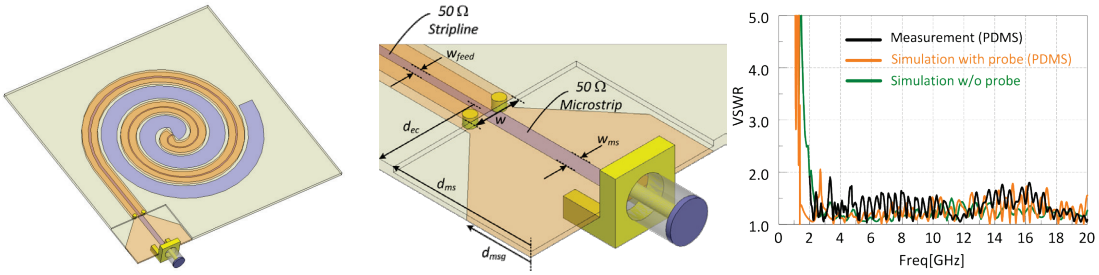

Fig. 8 (Left) CAD model of the stripline-based spiral antenna with a 90 linearly-tapered impedance transformer, (middle) feed section for the transition of the coaxial probe to microstrip, and microstrip to stripline, and (right) results for fabricated and simulated structure.

This project has also demonstrated the ability to integrate distributed circuit components into the shielded regions of an antenna, and that these can be realized without any major impact on antenna's performance. An edge-coupled 4-pole stripline band-bass filter was chosen for this purpose using the antenna and feed section illustrated on left diagram in Fig. 8. This filter was integrated into the linear feed section of the spiral first (e.g., 'outside the antenna'), and then into the curvilinear spiral to study the impact of forcing the filter to remain conformal to the topology of the spiral antenna (e.g., 'inside the antenna'). The band-pass frequency was designed for operation at 9.75 GHz using analytical techniques, and was not optimized after initial simulations to gauge the impact from the finite-ground in the stripline configuration first (for the antenna 'outside the antenna') and then the added influence of the structurally-modified design (for the antenna 'inside the antenna'). Fig. 9 shows the CAD model of both designs and the simulated VSWR of the two antenna structures.

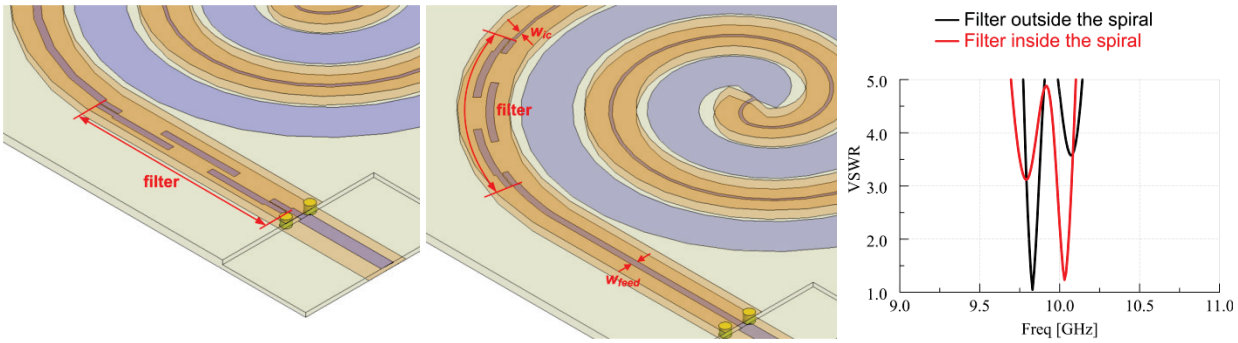

Fig. 9 CAD model of the stripline-based spiral antenna with the stepped band-pass filter (left) 'outside the antenna') and then (middle) 'inside the antenna'; (right) the simulated VSWR for both configurations.

Achievement 1.2.b *Integration of an impedance transformers into an inward-fed radial dipole*
PI: Gregory H. Huff
Undergraduate Student: Amanda M. Couch (Electrical and Computer Engineering)

An inward/externally-fed radial dipole antenna with an integrated broadband impedance transformer was investigated in this project through an undergraduate research program. This involved the study of complementary structures that could reside in a thin disc-shaped topology. Fig. 10 shows the simulated model, and experimental prototype, and measured results for the circular disc-shaped structure that was fabricated using 4mm thick Chloroplast (corrugated plastic) sheets with a 0.9144 m (36 in) width; this constrained the maximum diameter of the circle inscribing the radial dipole, and thereby the lower-bound of the bandwidth of the dipole mode, but the results indicate the potential of the concept. The antenna follows the stripline configuration being used for spirals (discussed earlier in this Thrust). The deviation in measured and simulated results is attributed to fabrication of the antenna. Specifically, this comes from the coaxial probe excitation and the connection of a fence of vias in the vicinity of the probe's connection to the inwardly-tapering impedance transformer through the Coroplast to provide continuity between the top and bottom grounds. Simulated results demonstrate the sensitivity of the geometry to these changes.

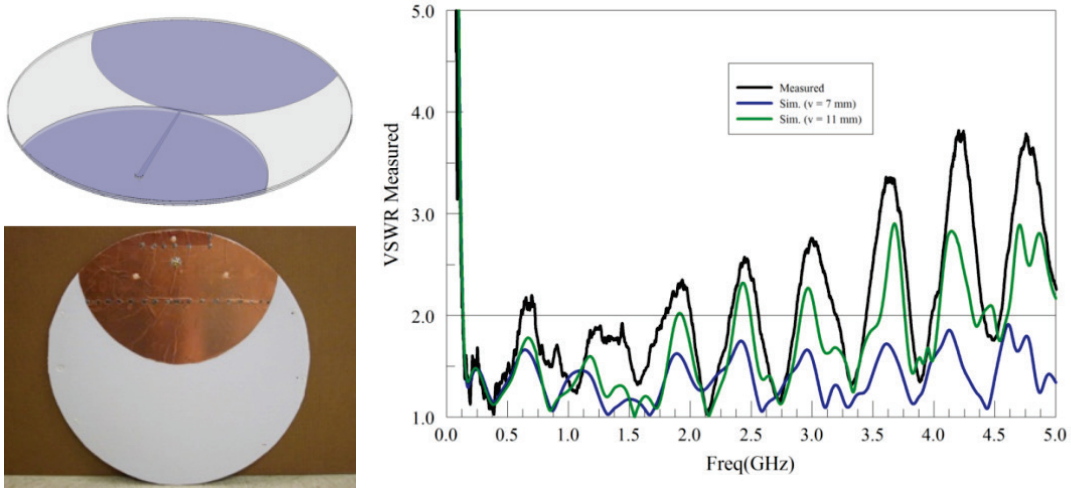

Fig. 10 (Left) Simulated and (right) fabricated internally-fed radial dipole antennas and (Right) measurements along with simulations results for the intended antenna and variations to show the cause of the impedance behavior observed in the measured results.

Outreach Objective 1 Design an Aperchassis (structurally functional antenna) suitable as a hand-launched UAV demonstration vehicle with practical physical constraints and realistic mission objectives

Outcome 1.1. An Android-based communication and control system for hand-launched UAVs
PI: Gregory H. Huff
Undergraduate Student: Amanda M. Couch (Electrical and Computer Engineering)
Undergraduate Student: Logan Dennison (Electrical and Computer Engineering)
Undergraduate Student: Giancarlo Galina (Aerospace Engineering)
Undergraduate Student: Michael Young (Aerospace Engineering)
Undergraduate Student: Leticia Ibarra (Electrical and Computer Engineering)

A multidisciplinary undergraduate student research group pursued the aerodynamic, electronic, and electromagnetic design of a new aerodynamically functionalized antenna prototype based on the fusion of a 'Nutball flyer' and a spiral antenna. Fig. 11 shows a prototype of the final system that was constructed for this. This design uses a Rohacell 71 HF (low-loss structural foam) with a diameter of 48 in. The platform features aerodynamic control surfaces which allow the craft to stand and take off vertically, perform several modes of flight, and hover. The Android smartphone system was connected to a nine-axis inertial measurement unit (IMU) through an Arduino microcontroller and a 433 MHz transceiver. This was connected to a receiving station on a laptop with a similar transceiver connected to a remote server, which provides data on the state of the UAV to an application on an Android smart phone.

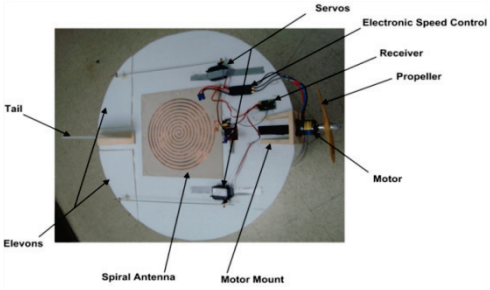

Fig. 11. Spiral antenna mounted to a flying wing UAV.

Outcome 1.2. Multifunctional materiel enhancement strategies for structurally functionalizing a load-bearing aerodynamic antenna platform
PI: Gregory H. Huff
PhD Graduate Student: Frank Drummond

A number of multifunctional material enhancement strategies have been pursued in this project. This includes the development material synthesis techniques and methods to evaluate the trade-offs related to material enhancement strategies. The analysis in this project considered the weight and strength of the material since they are assumed to play a shared role as the load-bearing (and flight-enabling) components of the antenna-based UAV. These parameters are linked to the antenna performance metrics through their dielectric loading, losses, and impact on physical size. The spiral and tapered slot have been used as the base antenna design. The material and aerodynamic design spaces are integrated together through this approach by establishing a set of aerodynamic constraints for the platform (lift, propulsion, etc.). These are embedded into the weight and stiffness of a composite, which is chosen to act as the antenna substrate and superatrste to strengthen the UAV body. The embedding of nanoparticle inclusions into structural foam was considerd in this project, and the candidate inclusions for the foam matrix were E-type fiberglass and rutile (both particle types are assumes to be mixed

randomly and have high particle aspect ratios resembling short sections of nanofibers). The rationalle for these materials was that foam is a low strength low dielectric constant host material, rutile (TiO_2) has high dielectric constant and good strength but high density, and fiberglass has lower dielectric constant but lower density and good strength properties. The illustration on the left side of FIG show a periodoc unit cell used to stufybthe multodiciplinary design objectives. The control parameters of interest were the electrical (dielectric strength ε_r) and mechanical (density ρ, Young's Modulus E, Tinsile Strength T_S, and Compressive Strength C_S), and the baseline effective medium properties were calculated using classical mixing formulas (Maxwell-Garnett) assuming all nanoparticles were randomly alighend and homogeniously mixed in the material matrix.

Weight limits were also added to better encapsulate the design space and provide a more realistic set of design constraints. The weight of materials, components, and other items considered essential (similar to the components in Fig. 10) were used to provide a base-line number for this purpose. Fig. 12 shows an example of a design optimization study to find the volume fraction of structural fiber and electromagnetically dense nanoparticle. A series of multi-physics simulations were also perfromed on the unit cell to better understand the performance of the nanoparticle inclusion and how they impact the design space of the antenna. This anaysis represents a key step in integrating the multifunctional material properties into the aerodynamic and electromagnetic design space, and illustrates a very unique approach for the design a of resource-constrained aerodynamically-functionallized antenna.

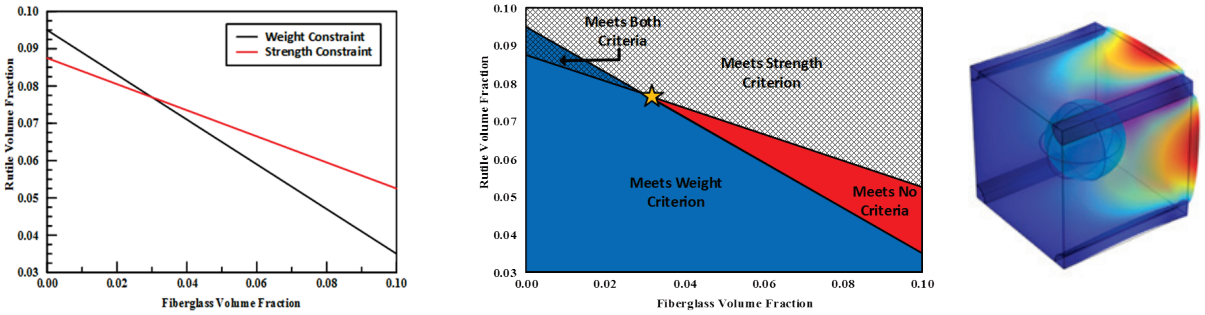

Fig. 12. Design curves for weight constrained and strength constrained cases as a function of composite composition (left), resulting representation of the design space this creates (middle), and periodic unit cell of E-type fiberglass and spherical nanoparticles used to determine multifunctional composite capabilities (right).

<u>Outcome 1.3.</u> Integration of control surfaces and other aerodynamic components on the electromagnetic performance of the structurally functionalized antenna.
PI: Gregory H. Huff
PhD Graduate Student: Frank Drummond
Undergraduate Student: Michael Young (Aerospace Engineering)
Undergraduate Student: Leticia Ibarra (Electrical and Computer Engineering)

The aerodynamic performance of a number of flying-wing designs were studied in this project. The goal of this was to determine the impact of intregrating different families of control surfaces onto the antenna platform. Fig. 13 shows two basic designs (labeled "Design A" and "Design B"). Design A has rudder and elevon control, and includes large vertical stabilizers to tunnel airflow into the elevator area. Design B has Wing dihedral to increase roll stability at low speeds, a larger motor mount for increased structural stability, and both rudder and elevator control. ***FIG*** also shows the simulated lift (middle) and drag (right) for each design at two different air speeds (5 mph and 20 mph) over an angle of attack from 0° to 50°. Both of the designs have comperable aerodynamic performance are capable of sustained hovering-in-place using the rudder and elevator/elevon to counteract motor torque and each have a high degree of agility. The designs differ slightly in the wing design, but Design A also features a rudder

and elevon configuration which allows it to perfrom verticle take-off and landing. The impact on antenna performance from the placement and orientation of control surfaces on the load-bearing antenna were minimal.

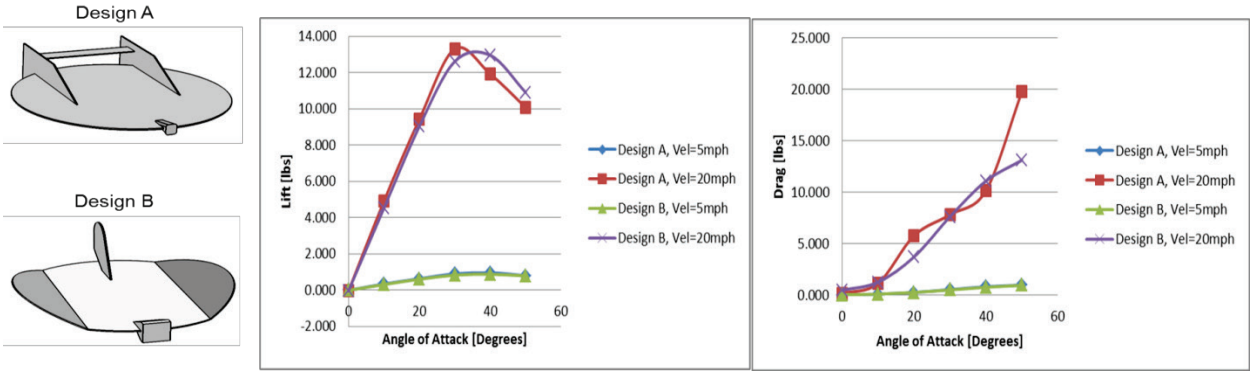

Fig. 13 Design CAD models for two variations of flying wing design (left), and simulated lift (middle) and drag (right) for two different flight speeds.

Outcome 1.4. Design and fabrication of a micro air vehicle based on the multifunctional design approach
PI: Gregory H. Huff
PhD Graduate Student: Frank Drummond
Undergraduate Student: Deana Sessions (Electrical and Computer Engineering)
Undergraduate Student: Lisa Smith (Electrical and Computer Engineering)

The aerodynamic functionalization of a broadband antenna design and integration of subsystems onto this structure for flight-testing and other experimental activities was pursued in this project using a micro air vehicle. The screenshots in Fig. 14 show the aerodynamically functionalized antenna (similar to Fig. 10) that was constructed. It is based on a circular flying-wing structure (referred to in the hobbyist community as a "Nutball flyer"). This design was chosen since it provides 1) stable, low speed flight with agile maneuverability in high traffic areas, 2) a structure that is capable of vertical take-off and landing (VTOL), 3) a platform that can hover to maintain a current position, and 4) a large surface area for mounting electronic systems and supporting systems. This particular design was fabricated using 3D printed components from ABS and a stripline-based radial dipole/tapered slot antenna fabricated on a Duroid 5880 substrate. The measured electromagnetic and simulated aerodynamic performance results are provided in Fig. 15 and Fig 16, respectively. The design was not optimized, but the results indicate that the integrated design process developed in this project was successful, and it has the possibility of being refined using a full multi-physics analysis tool.

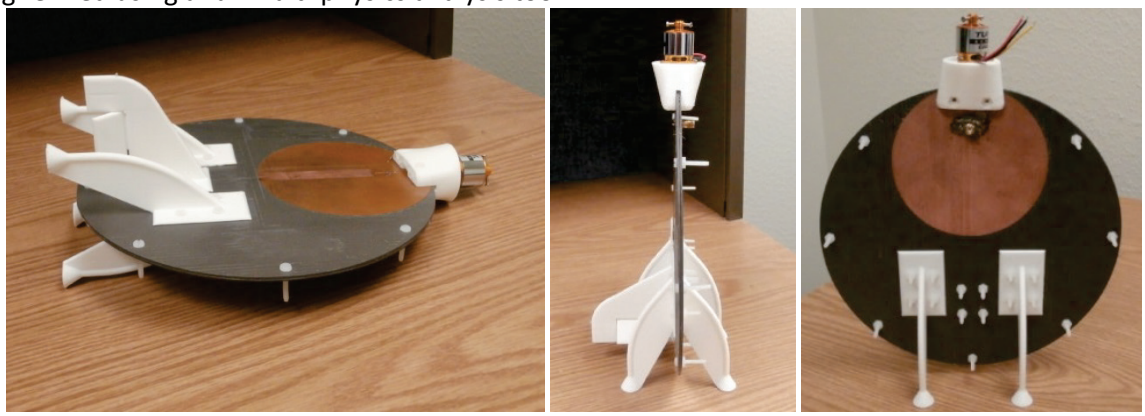

Fig. 14 Fabricated prototype of the MAV based on an aerodynamically-functionalized antenna.

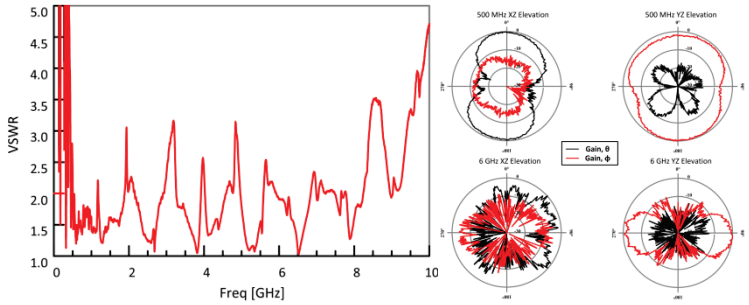

Fig. 15 Measured VSWR (left) and radiation patterns (right) of the first MAV prototype developed to study the co-design of electromagnetic and aerodynamic capabilities.

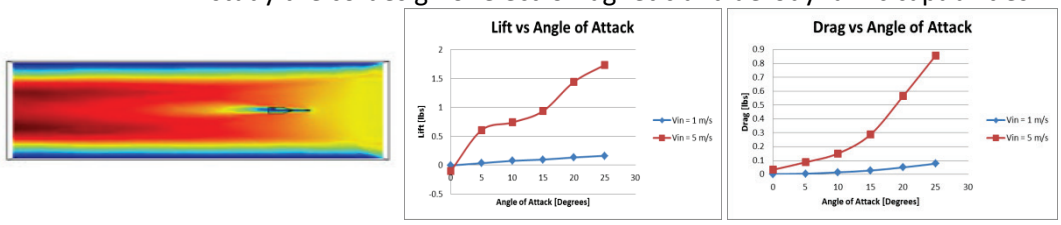

Fig 16 Wind tunnel simulation (left); lift (middle) and drag (drag) as a function of angle of attack for the aerodynamically functionalized MAV design.

<u>Thrust 2</u>: Antensors – Investigate the fusion of mm-wave apertures and dense sensor arrays as integrated EM and structural reconfiguration mechanisms

<u>Research Goal 2.1</u> Multiscale integration techniques that facilitate the reconfiguration of traveling wave antennas through the integration of dense and dynamic sensor arrays

<u>Achievement 2.1.a</u> *Multi-physics design of a multifunctional mode converter, vortex-flow conditioning, and impedance transformer for a traveling wave antenna*
PI: Gregory H. Huff
MS Graduate Student: Loizos Loizou

A broadband mode-converting transition between a rectangular waveguide (RWG) and a trough waveguide (TWG) has been designed, fabricated, and successfully tested. The structure provides minimal impedance mismatch and mode conversion across an entire waveguide band. Fig. 17 shows the CAD model and two back-to-back RWG-to-TWG transitions of length L and a metal thickness t that remains uniform throughout the structure. The outer perimeter of the transition provides a linear taper between the RWG and TWG. Flaring between the top and bottom walls remains symmetric about the center fin and flaring between the side walls is upward-directed to maintain a flat mounting surface at the bottom of the structure. The septum (center fin) tapers linearly from a height of zero at the RWG port to the fin height s at the TWG port in an upward direction from the bottom of the structure.

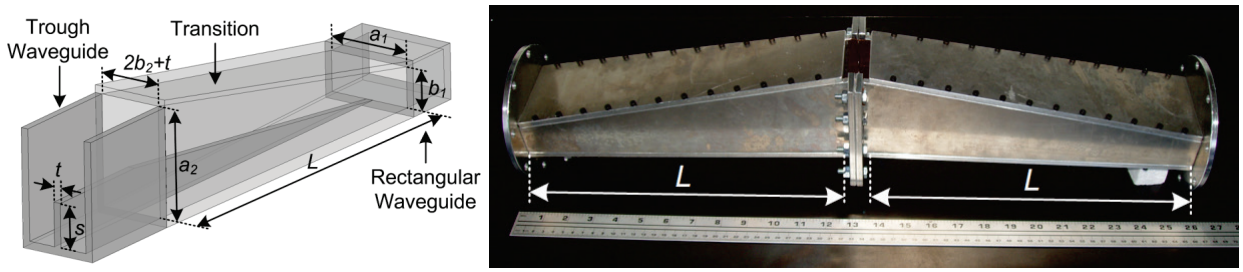

Fig. 17 (Left) CAD model of RWG-to-TWG transition and (right) back-to-back fabricated structures.

The left side of Fig. 18 shows the electromagnetic performance of a single transition that was de-embedded from the back-to-back structure using ABCD-matrix approach. Less than 0.8 dB of insertion loss was observed across the entire S-band. This structure connects to a trough waveguide antenna (TWA) with cantilever-based sensing and reconfiguration mechanisms. These sensors are intended to detect airborne contaminants, gaseous chemicals, and other aerosolized compounds so the air-flow in the structure was included into the design of the transition. Its multifunctional role is therefore to channelize the airflow into a turbulent within the troughs of the TWA to evenly disperse the contaminants along banks of sensors (to increase detection capabilities and decrease false positives). For this structure the maximum airspeed was set to 60 m/s as a way to emulate the speed of an unmanned aerial vehicle (UAV) or high-speed wind such as a tornado. To maintain this vorticity down at lower speeds the structure had to be lengthened; this created a smoother transition for the electromagnetic functionality and did not impact its performance negatively. This illustrates the ability to design a multifunctional structure using a multi-scale and multi-physics approach.

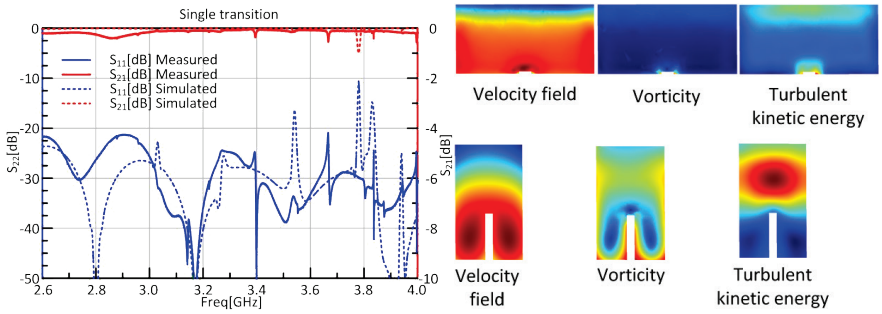

Fig. 18 (Left) Electromagnetic and (right) aerodynamic performance of the RWG-to-TWG transition at the input section of RWG (top-right) and output section of the TWG (bottom-right).

Achievement 2.1.b *A design methodology and synthesis technique for enabling reconfigurable radiation from a traveling wave antenna using dense sensor networks*
PI: Gregory H. Huff
MS Graduate Student: Loizos Loizou

Reconfigurable radiation behavior from a trough waveguide antenna using a concept for a dense sensor network was demonstrated in this project. The specific properties of the sensing system were not considered for the fundamental electromagnetic design and synthesis problem, but it is assumed that arrays of small cantilevers with embedded sensing mechanisms are densely packed along both sides of a TWG. Radiation is facilitated using this sensor network by actuating the cantilevers in a periodic antipodal distribution to synthesize the desired effective aperture distribution. This concept is based on the ability to perturb an open/leaky structure to enhance and control the resulting radiation properties. The left side of Fig. 19 shows the simulated electric field structure of the TWG; the middle and right images in this figure are included to illustrate the impact of cantilever size on the effective aperture.

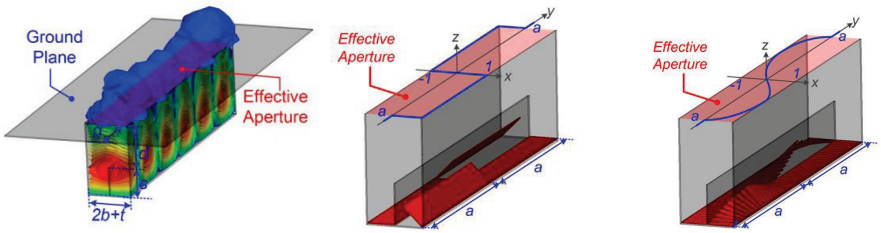

Fig. 19. (Left) Electromagnetic field in the trough waveguide antenna, (middle) unit cell using large cantilever to obtain a rectangular antipodal effective aperture distribution and (right) unit cell using small cantilevers to obtain a sinusoidal-tapered antipodal effective aperture distribution and.

An analytical model has also been created to study the frequency-dependence of the main beam, grating lobes, aperture tapering, and the side-lobe distribution. This includes the discretized approach to synthesizing the desired effective aperture by actuating the cantilevers in the TWG; this provides the ability to study the impact on tapering and other beamforming capabilities. Fig. 20 shows the calculated results from this model for an effective aperture (TWA), and Fig. 21 shows the finite-element simulations of a W-band TWA with an aperture length of 40mm. In each of these plots, the left diagram shows a 2mm cantilever length, the middle diagram shows a 4mm cantilever length (half of a guided wavelength in the TWA at 95 GHz), and the right diagram shows a 5mm cantilever length. Fig. 21 includes the frequent-dependent scanning of the beam for each cantilever length. This model provided an accurate representation of the radiation behavior, and provided a method to synthesize a desired aperture pattern for the structure.

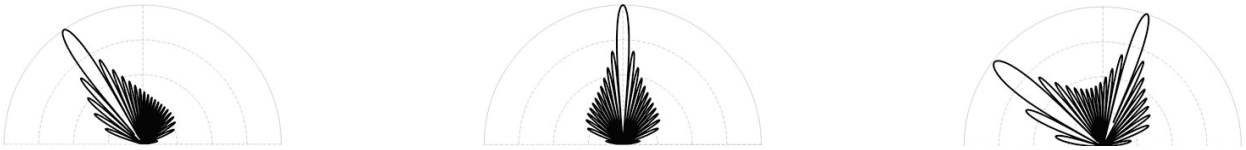

Fig. 20. Calculated radiation behavior for (left) a quarter-wave, (middle) half-wave, and (right) five-eighths-wave cantilever lengths.

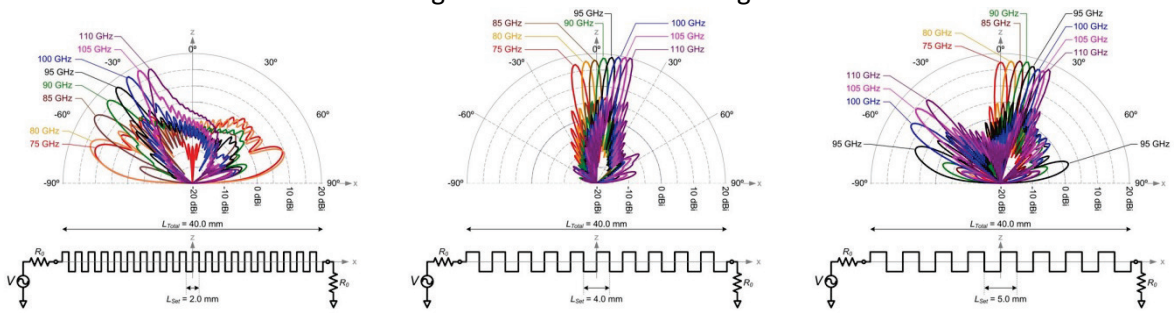

Fig. 21. Simulated radiation behavior across W-band for (left) a quarter-wave, (middle) half-wave, and (right) five-eighths-wave cantilever lengths.

Achievement 2.1.c *Demonstration of beam steering and compensation of phase accumulation and reactive loading to steer a traveling wave structure through broadside*

PI: Gregory H. Huff

MS Graduate Student: Loizos Loizou

One of the key limitations a traveling wave antenna of this variety is the phase accumulation that occurs when the bean is scanned through broadside. This loading is capacitive, and this project proposed a general methodology to compensate for this behavior. The cantilever perturbation is used to demonstrate this concept with circular apertures cut into the cantilever to create an inductive loading mechanism on each cantilever that compensates for this capacitive effect. The aggregate result is that the compensation mechanism maintains a suitable impedance match for the structure. An S-band prototype TWA Antensor was designed and fabricated; measurements were performed to validate the proposed method. Fig. 22 shows the layout of the half-wave cantilevers (outside the TWA) and the image of the original and modified cantilevers (e.g., with and without the inductive apertures). Fig. 23 shows the radiation and impedance behavior of the half-wave cantilever both with and without the compensation mechanism. This illustrates the effectiveness of the general method. Fig. 23 shows that at this frequency, the antenna experiences phase accumulation and the circular apertures provide a compensating reactive loading that allows the structure to maintain its impedance match when scanning through broadside.

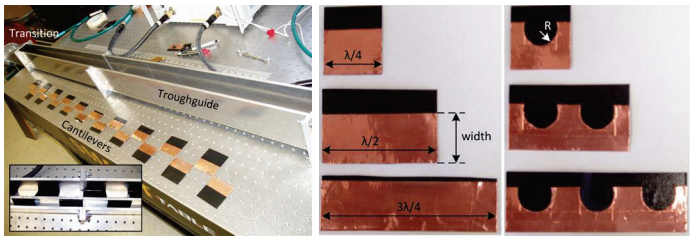

Fig. 22. Measurement set-up for impedance testing of the TWA and the cantilevers with circular aperture tuning mechanisms.

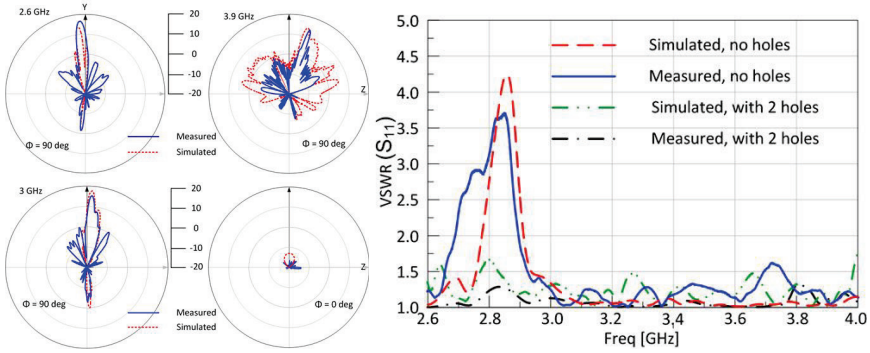

Fig. 23 Measured radiation (Left) and VSWR (right) of the half-wave cantilever both with and without the compensation mechanism.

<u>Research Goal 2.2</u> Advanced analytical models based on the multi-modal decomposition of traveling-wave antennas, variational techniques, and a novel use of the Compensation theorem

<u>Achievement 2.2.a</u> *Latticed-based circuit model of frequency selective surfaces*
PI: Gregory H. Huff
PhD Graduate Student: David Rolando

A semi-analytical technique suitable for both analyzing and synthesizing frequency selective surfaces (FSSs) was developed in this project. This analysis can be used for synthesis, and it is applicable to higher-order/multilayer structures and reconfigurable designs. The analysis relies on establishing an equivalent circuit of the FSS which includes mixed-order coupling to adjacent elements to develop an N-port representation of the periodic cell, then applying a periodic Green's function to solve the lattice formed by the self and mutual impedances. The process is analogous to deriving the active impedance of an antenna in an array to determine scan blindness, and the basic steps are outlined in Fig. 24 for a nominal circular aperture.

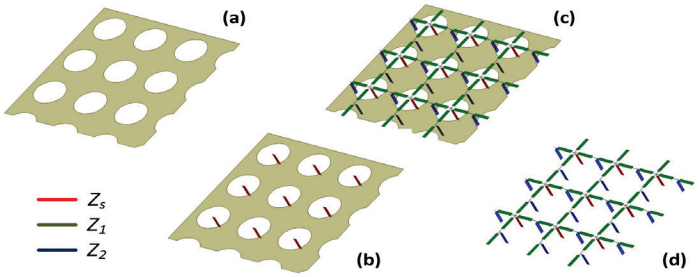

Fig. 24. Conceptual development of lattice-based circuit model for FSS: (a) the physical design, (b) the aperture self-admittance, (c) the first and second order elements, and (d) the equivalent circuit.

This analysis process is capable of being coupled to an optimization routine and used for synthesis. In this process, it is possible to constrain the unit cell size and/or define a target pass-band, stop-band, etc.

The two FSS topologies in Fig. 25 were used to evaluate this method for resonant rectangular apertures to create single- and dual-band pass-band FSS. The measured, simulated, and modeled results (using the process developed in this project) for each geometry can be seen in Fig. 26 and the agreement is good between simulated (HFSS) and modeled. A frequency shift can be seen in the measured results, and these deviations in experimental observations are attributed to the test fixture and free-space calibration procedure used in measurements. This semi-analytical formulation has also been used to create electromagnetic windowing using reconfigurable FSS.

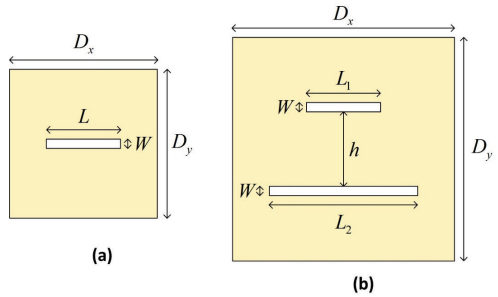

Fig. 25. Geometry of rectangular aperture FSS. (a) Single-aperture design and (b) dual-aperture design.

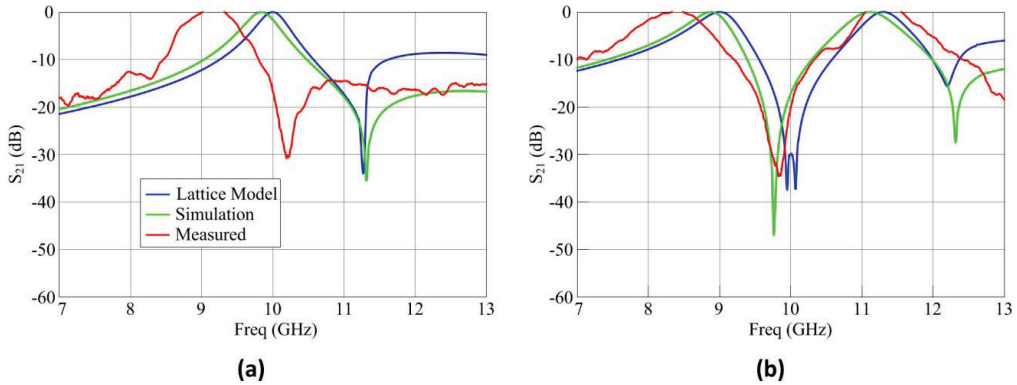

Fig. 26. Measured, calculated, and simulated transmission of the optimized (a) single rectangular aperture FSS and (b) dual rectangular aperture FSS operating in the X-band.

Achievement 2.2.b *A partial-hemisphere cavity model for spherical microstrip-based antenna topologies*
PI: Gregory H. Huff
PhD Graduate Student: David Rolando
MS Graduate Student: Jacob McDonald

A spherical inverted F-antenna was investigated in this project as a multifunctional antenna platform for unattended ground sensor platforms (UGS). A partial-hemisphere cavity model was developed to characterize its performance and provide physical insight into its design and operation. Fig. 27 shows a graphical representation of the cavity formed by perfect electrical conductor (PEC) and perfect magnetic conductor (PMC) walls. A geometric transform (similar to conformal mapping) was used to create a custom coordinate system to analyze this cavity; it is given in coordinates *u*, *v*, and *w*, where *u* is a linear quantity and *v* and *w* are angular quantities. Fig. 27 shows the results from a basic transmission line model, the aforementioned cavity model, finite-element simulations, and measurements of the fabricated antenna designed for 400 MHz. This treatment of the antenna accurately predicts both the impedance and radiation behavior of the antenna, and the model provided a unique demonstrate of fractional modal parameters (a novel and emerging topic in fractional calculus).

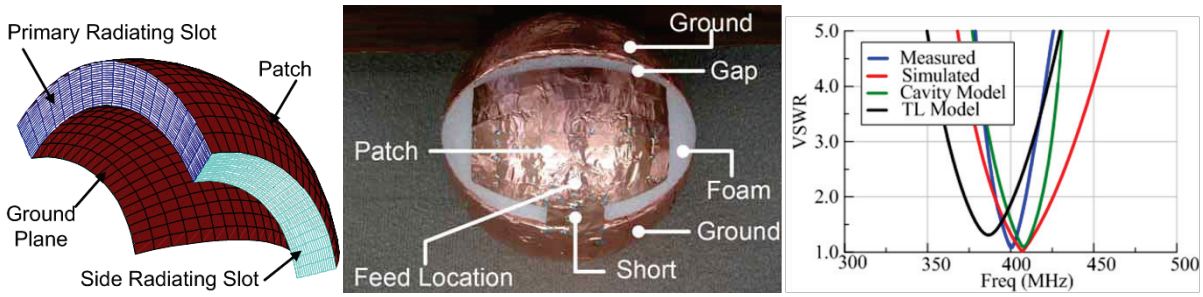

Fig. 27. Cavity model, fabricated antenna, and VSWR of the SIFA designed for 400 MHz.

Outreach Objective 2 A radiation reconfigurable W-band antensor using a deformable cantilever arrays as the sensor-based reconfiguration mechanism for SAR.

Outcome 2.1. A W-band radiation-reconfigurable trough waveguide antenna using a liquid metal reconfiguration mechanism
PI: Gregory H. Huff

The experimental work discussed earlier in this Thrust was limited to S-band designs due to fabrication and measurement constraints, but it provided a basis for exploring more complex designs spaces to facilitate reconfigurable radiation from the TWA. The pressure driven displacement of liquid metal EGaIn perturbations in a metallic TWA was considered for this. Several designs were simulated to develop a better knowledge base on the use of the fluidic system to perturb the structure. A screen shot for this new concept in reconfiguration has been included in Fig. 28. This image shows the small fluidic sections in place of the cantilevers in Fig. 19, where periodic 'droplets' provide the antipodal perturbation. Fig. 29 shows the impedance (left) and radiation pattern at broadside (right) at 93 GHz– these plots are included to verify the basic behavior of the structures is maintained using this new type of. The key observations from these results are that the use of new reconfiguration technologies can be applied to facilitate reconfigurable antenna behavior at mm-wave frequencies .

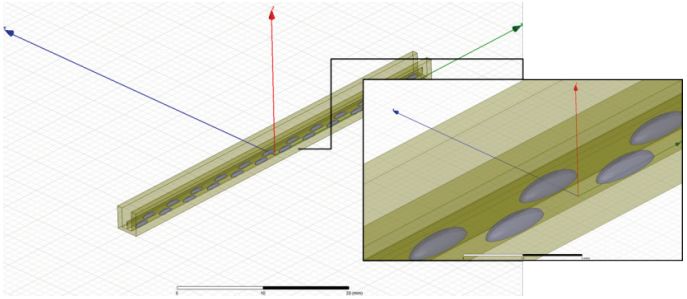

Fig. 28. Screenshot of CAD (HFSS) model for the W-band troughguide antenna using liquid metal perturbations.

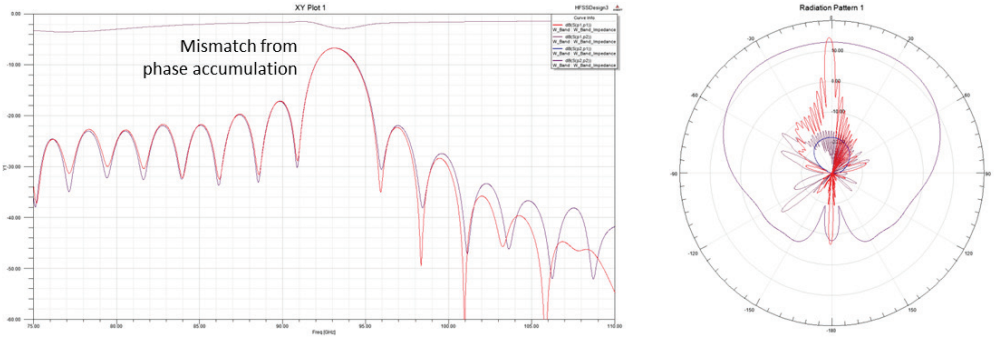

Fig. 29 Simulated impedance (left) and radiation (right) of the W-band TWA antenna using liquid metal perturbations to enable reconfigurable radiation behavior.

<u>Thrust 3</u>: Collaborative Techniques - Provide the analytical framework for dynamic networks of Aperchassis with integrated Antensor technologies

<u>Research Goal 3.1</u> Beamforming techniques for morphing networks that apply principles from random and space-tapered arrays to optimize the performance and constrained power-budgets of highly mobile arrays of independent platforms

<u>Achievement 3.1.a</u> A comprehensive mathematical framework for random/unstructured arrays
PI: Gregory H. Huff
PhD Graduate Student: Kristopher Buchannan

This project has developed an extensible mathematical framework for analyzing the fundamental properties of random arrays based on the Fourier transform techniques. This general technique has been widely used in similar theoretical descriptions of other array topologies. However, this project has worked towards the development of a theory that can be unified and applied to the problem space of generalized volumetric random arrays. The spherical distribution of elements shown in Fig. 30 provides the general context for this analysis. This figure shows a spherically bound random array; it is assumed to be a cluster of *N* isotropic radiators that are bound by a spherical volume of radius *A*. This sphere is defined by the cluster's center, taken as the origin *O*, and the outer-most radiator(s) on the spherical surface (this ability for inclusiveness is a key feature of this analysis).

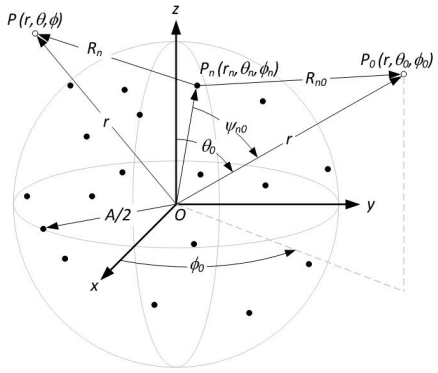

Fig. 30 Random distribution of elements in a spherical volume.

The following practical considerations and mathematical assumptions arise in this context: 1) the synchronization amongst sources is assumed sufficient for high-fidelity phase control or time delay with negligible degradation from frequency offsets or phase jitter, 2) the sources are uniformly distributed within the volume of interest, 3) all sources have equal power and all signals experience equal path losses, 4) there are no reflections or scattering that will introduce multipath, fading, or shadowing, and 5) all elements are sufficiently separated to ignore mutual coupling. It is assumed in this mathematical treatment that these conditions are achieved such that the array can coherently add signals in the desired direction and randomize them to the extent that a net destructive interference occurs in all other regions. The process for analyzing these arrays is summarized here, and begins by defining the generalized array factor *F*, This is shown in the equation below.

$$F\left(\theta,\phi\left|r_n,\theta_n,\phi_n\right.\right)=\frac{1}{N}\sum_{n=1}^{N}e^{j\vec{k}\cdot\left(\vec{R}_n(\theta,\phi)-\vec{R}_{no}(\theta_o,\phi_o)\right)}\approx\frac{1}{N}\sum_{n=1}^{N}e^{jkr_n\left(\cos\psi_n-\cos\psi_{no}\right)}$$

This is followed by defining the normalized radiation intensity *U* shown below.

$$U\left(\theta,\phi\left|\vec{r},\vec{\theta},\vec{\phi}\right.\right)\overset{Normalized}{=}\frac{1}{N^2}\sum_{n=1}^{N}\sum_{m=1}^{N}e^{jkr_n\left(\cos\psi_n-\cos\psi_{no}\right)}e^{-jkr_m\left(\cos\psi_m-\cos\psi_{mo}\right)}$$

Lastly, the expected power pattern is found by considering the spatial functions in the previous expression as joint random variables. This leads to a key result of this work: the mean valued radiation intensity is composed of two distinct terms, the main lobe factor and the average side-lobe level.

$$\overline{U}(\theta,\phi)=\frac{1}{N}+\left(1-\frac{1}{N}\right)\left|\Lambda\right|^2=\text{Average Sidelobe Level + Mainbeam}$$

$$\Lambda=\left[\text{MainLobeFactor}\right]=\left[\text{Characteristic Function}\right]$$

This analysis provides a similar, but more extensible form of the array factor in previously derived analysis of random arrays. The key to this analysis is understanding the importance of the characteristic function, and an extensive amount of work was performed in this project to link this main lobe factor into the SNR, beam width, and other fundamental properties of arrays. Potential examples where this theory can be applied include static and quasi static environments such as radiating nodes dropped from an overhead aircraft, micro air vehicle (MAV) clusters, and space-borne constellations of nano-satellites. Additional constraints from the host platform dimensions, an accurate estimation of position and location information, and adequate synchronization are also extremely important considerations in each of these scenarios (and many other illustrative examples of interest to the authors of this work), but in most cases these platforms are constrained in the power resources they have available for transmission. Thus, in an autonomous operational framework, the theory in this work can be applied for beamforming in a collaborative network to determine which agents in a given volumetric configuration are required for beamforming and which can remain active on in a networking role.

This provides a unique way to facilitate long back-haul wireless relays of information from these types of networks, and places less constraints on the bandwidth and information content which can be encoded in advanced modulation schemes with direct digital synthesis (DDS) architectures. The analysis also shows that a directivity of order N is achieved (with an appropriately narrow beam) as long as the element distribution remains sufficiently sparse. In addition, it has been shown that a spherical volumetric array will on average produce lower side lobes than its two-dimensional circular counterpart at the expense of a broader main beam. Even more, it is seen that the law of large numbers holds and describes these expected power pattern as a convergence resembling the definition of an average defined from the context of probability as the number of elements increases to infinity (Fig. 31).

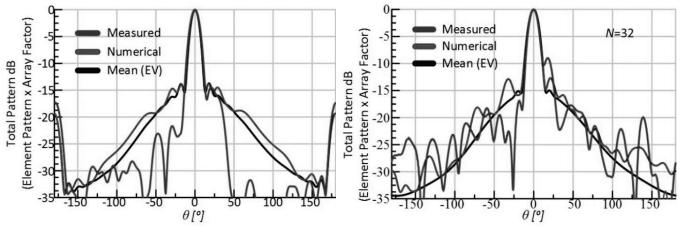

Fig. 31 Simulated and experimental results of CRA (left) and SRA (right).

Achievement 3.1.b *A modular controller and smartphone application for automating phased arrays and tethering them to peripheral applications*
PI: Gregory H. Huff
PhD Graduate Student: Jeffrey S. Jensen

A modular controller and smartphone application was developed in this project to experimentally evaluate the radiation characteristics of circular and spherical random arrays. The controller receives antenna element positions from data sources (smartphone) and the intended scan location, as this is needed to determine correct phase shifting for individual elements. Control signals are generated which adjust the phase in phase shifter elements thereby steering the beam of the array. The controller is

capable of calculating phase shifts for two-dimensional and three-dimensional arrays and communicates with the smartphone using Bluetooth or Wi-Fi. The compact design features high precision phase control with 16-bit accuracy and controls up to 48 individual phases. Additionally, the controller can receive GPS coordinates from other mobile devices, such as a smartphones and UAVs, allowing the controller to steer the main beam to follow these devices using tracking algorithms. This is extremely useful for implementing spatial security access, load balancing, and communication quality. Furthermore, the controller provides a cognitive platform capable of programming several different types of radiation patterns mentioned in this work such as sum-difference, endfire and broadside radiation patterns. It is also capable of connecting external data sources, such as position and image data that help minimize any error in determining element position or phase errors. Fig. 32 shows the system diagram, and Fig. 33 shows one modular unit of the controller as well as the fully assembled control system and RF manifold.

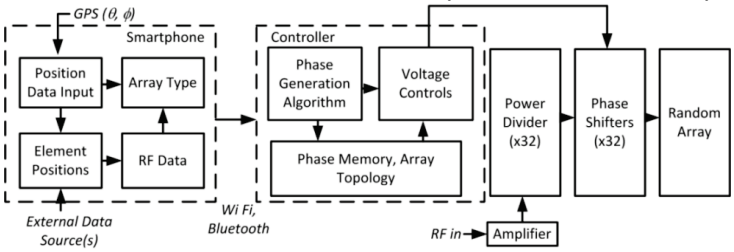

Fig. 32. Modular array controller architecture and system diagram

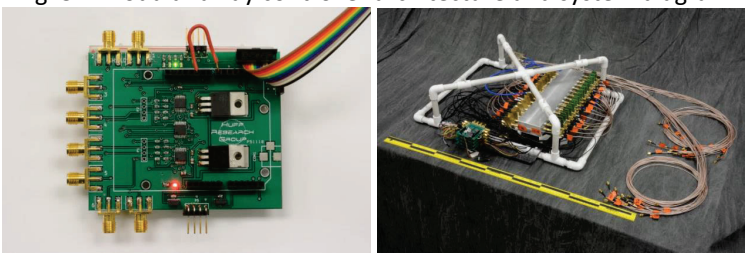

Fig. 33. Single modular control board used for experimental study (left) and assembled control system with RF distribution network (right).

Outreach Objective 3 Aperture partitioning in a high-low network combines the functionality of the previous two thrusts and considers the physical impact of a dual-band (high-low) network architecture (HF and W-band) for beamforming and local networking.

Outcome 3.1. *Beam steering and aperture partitioning in random arrays*
PI: Gregory H. Huff
PhD Graduate Student: Kristopher Buchannan
PhD Graduate Student: Jeffrey S. Jensen
Undergraduate Student: Ryan A. Brown
Undergraduate Student: David Grayson

This project has examined the array behavior of randomly distributed antennas in linear, planar, and volumetric element distributions. A particular emphasis was placed on demonstrating a high degree of pattern control, and several spherical and planar random arrays were investigated to benchmark the theoretical analysis discussed in the previous discussion. Fig. 34 shows an example of the arrays that were examined experimentally. This includes a spherical random array with coplanar element placement of directional antennas (microstrip patches), collinear vertically-polarized omnidirectional antennas (monopoles), and planar circular random array (CRA) of microstrip patches. Fig. 35 shows the results from the planar thirty-two element CRA populated by microstrip patched operating in the 2.4 GHz ISM band. This was included to highlight the work in this project on aperture partitioning.

Fig. 34 Spherical random array with coplanar element placement (left), vertically-orientated monopole array (middle), and planar circular random array of microstrip patches (top-right) with smartphone controlled beamforming network (bottom-right).

In these experiments, the aperture was examined for its ability to provide simultaneous sum-difference pattern generation from interior and exterior elements in the array. The black and grey color of the inset circular diagram indicates the sum and difference modes of the partition, respectively, where the "+" and "-" illustrates the even and odd phasing, respectively, applied to each half of the interior and perimeter sub-arrays. With the exception of the full-sum and full-difference modes, each sub-array was measured with non-active elements replaced by matched loads. It is observed that well behaved sum and difference beam patterns may be obtained by either even or odd (anti-modal) types of distributions, which demonstrates the applicability of the analytical work and the use of the CRA as a partitioned aperture for simultaneous sum-difference pattern generation. The two spherical volumetric random arrays were also used to demonstrate scanning as well as sum-difference patterns. In addition to validating the theoretical components of this work, this experimental campaign provides the ability to observe the impact from blockage (as seen by elements in the interior region of the SRA).

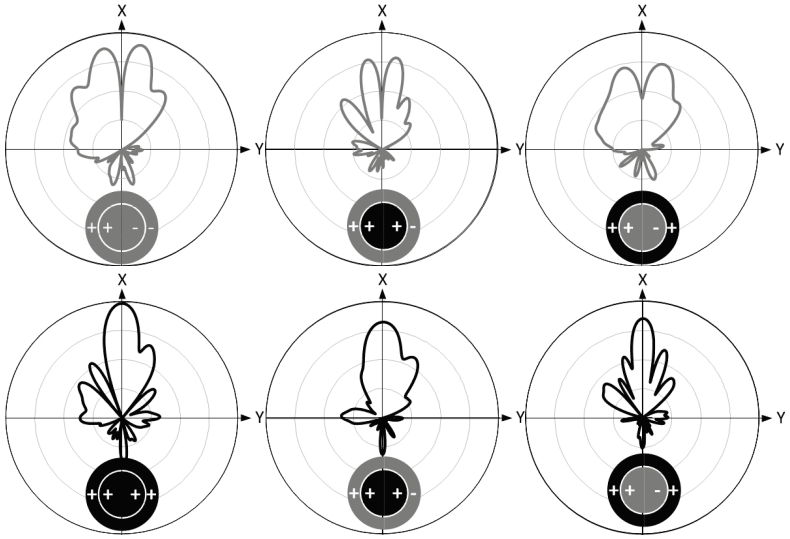

Fig. 35. Measured results from the partitioned CRA aperture in four phasing scenarios: full sum (lower-left), full difference (top-left), interior sum (lower-middle) with exterior difference (top-middle), exterior sum (lower-right) with interior difference (top-right).

This work has not only clarified the connection between the Fourier transform relation in random antenna arrays to the discrete Fourier transform in periodic antenna arrays, but has also added a significant contribution to the literature. In addition, both cosine and sine Fourier transforms may as well be utilized for sum and difference generation providing the random array greater multi-functionality. It has been shown under ideal conditions that the directivity of an aperiodic array topology

is capable of achieving directivities on the order of *N*, for sparse element arrangements. Periodic arrays are capable of obtaining directivities greater than this, but induce grating lobes while scanning. In addition, it has been shown that the resolution of a volumetric spherical random array is invariant of scan angle unlike scan behavior encountered in circular random arrays.

Outcome 3.2. *Computer vision assisted beamforming and geolocation of swarming antenna arrays*
PI: Gregory H. Huff
PhD Graduate Student: Jeffrey S. Jensen

A framework that utilizes open source computer vision tools and techniques to facilitate in-depth study of radiation characteristics of swarming antenna arrays was developed in this project. The system resolves spatial identification of elements (or platforms) and tracks the morphing spatial distribution to provide feedback and control information for phase shifting and beamforming. Core performance of the phased array control framework compares element phasing distributions and calculations to respective array radiation behavior. This begins with a discovery phase that leverages spatial detection algorithms to resolve element identities and analyze their relative locations within an optical field of view. Algorithms compress accompanying information from a depth-of-field sensor to evaluate the spatial distribution of elements and enable the tracking of element locations in time. Spatial information is used in a distributed array controller to calculate respective phases in the array to achieve desired beam steering functionality. User interaction through a mobile device (smartphone, tablet, etc.) is used to control the phased array and subsequently link geolocation information for autonomous tracking modes. A system and aperiodic array operating at 2.4 GHz was constructed using low-cost off-the-shelf components. Fig. 36 shows a diagram of the physical set-up and block diagram of the system. This includes the implementation of the computer vision assisted architecture that uses the depth and color images of a Microsoft Kinect to determine real world, Euclidean space coordinates for each element in a bound geometry. Calculations and post-processing of image data utilize various filtration and image correlation techniques to positively identify the element's location in reference to the bound geometry.

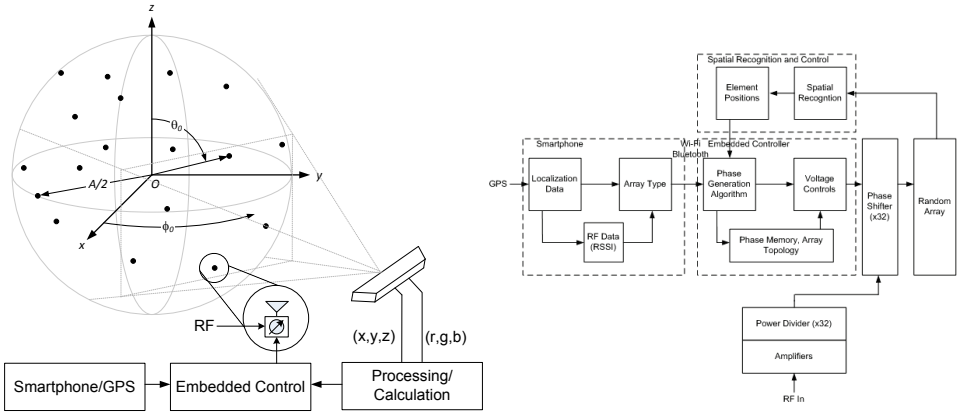

Fig. 36 Diagram of the physical set-up for the swarming array control framework (left) and block diagram of control network (right).

The system developed in this project aims to collaboratively synchronize electromagnetic information to overcome wireless synchronization challenges. One such issue that arises in wireless collaboration of morphing nodes in a swarming cluster is element location and the respective impact on the array's radiation behavior and capability. The scope of this effort therefore focused on a novel system that detects spatial configurations and provides element phasing within swarming arrays. The resulting autonomous phased-array control framework uses a Microsoft Kinect, its infrared spatial capabilities, and image processing algorithms as a useful and scalable platform for phasing control of swarming

arrays. Uniquely identifiable electromagnetic targets are considered for ease of use in the experimentation portion of this work. The systematic design of such targets to model real UAVs was also important in order to scale the proposed framework to be used in widespread UAV and distributed network applications. These synthetic UAVs are shown in Fig. 37; they include a patch antenna designed for 2.45 GHz that shares a substrate with embedded electronics typically found on a UAV. This includes a microcontroller, accelerometer, gyroscope, and Ethernet (wired) connection but is isolated from these DC components using a quasi-PEC through-hole via wall around the perimeter of the patch antenna (the Ethernet and wireless connection is meant to mimic the high-low network arcetecture). The embedded microcontroller regulates four red-green- blue (RGB) light emitting diodes (LEDs) at the four corners of the patch antenna upon receiving commands through the Ethernet network from a central control node.

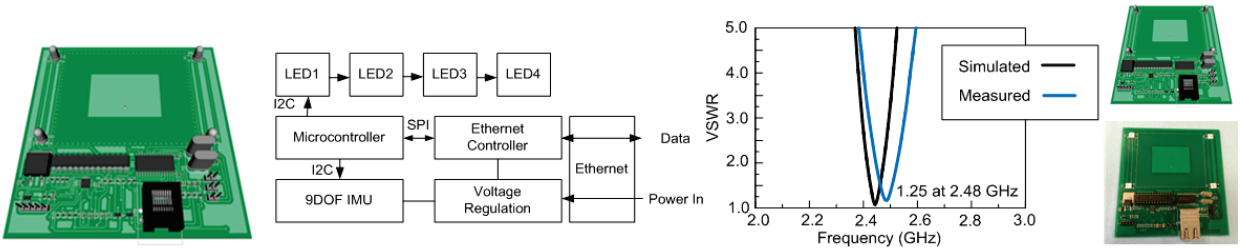

Fig. 37 (Left) Designed and (right) fabricated antenna element with onboard synthetic UAV platform.

The central processing control node of the framework issues identification commands to the antenna platforms and accordingly uses the Kinect to analyze RGB and depth image streams to resolve a specific antenna platform position in space. The detection and position estimation of the antenna relies on a series of image processing transforms that ultimately correlate a unique match or footprint of the antenna as shown in Fig. 38 .

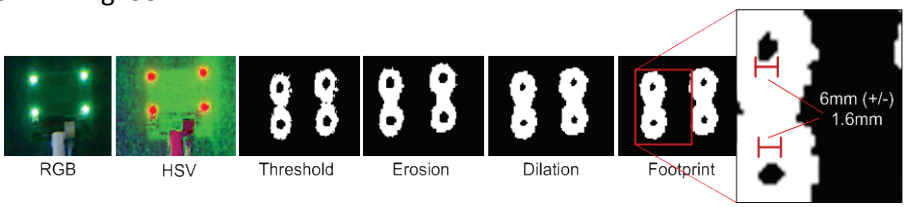

Fig. 38 (Left) Progressive image processing steps to determine antenna position.

A reticulating material was used to support each of the antenna platforms. This allowed each antenna to be moved to various positions within a bound volumetric geometry. Several geometries could therefore be quickly created, assessed, and tested to determine radiation characteristics, beam steering capabilities and other array behaviors. The central control system also uses the measured locations of each element through time to determine the characteristic function of the bounding geometry and incorporate functions such as tapering and dividing nodes into sub-arrays. Several volumetric geometries were configured by placing the elements in a pseudo-random design with the positions being completely unknown to the control system. Fig. 39 shows simulations from one of the configurations tested; this is representative of activities that were performed to identify and evaluate the error from phase shifter quantization and measurement/estimation uncertainty.

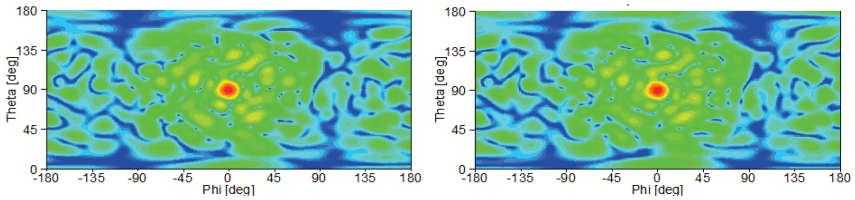

Fig. 39 Normalized gain of 32 element random array (left) with no error (right) 4-bit random error

Fig. 40 shows the phased array apparatus that supports up to 32 elements. This was created in this project to test motion-dynamic swarms using the framework as shown in Fig. 36. A large number of experiments were performed in this project using this test apparatus. Results show accurate alignment of the main radiation beam, and an error of 1.2% when steering the main beam. Fig. 41 shows an example of these experiments (taken using the set-up shown in Fig. 40). It is important to note that the average side-lobe level is higher in the measured patterns when compared with the simulation patterns.

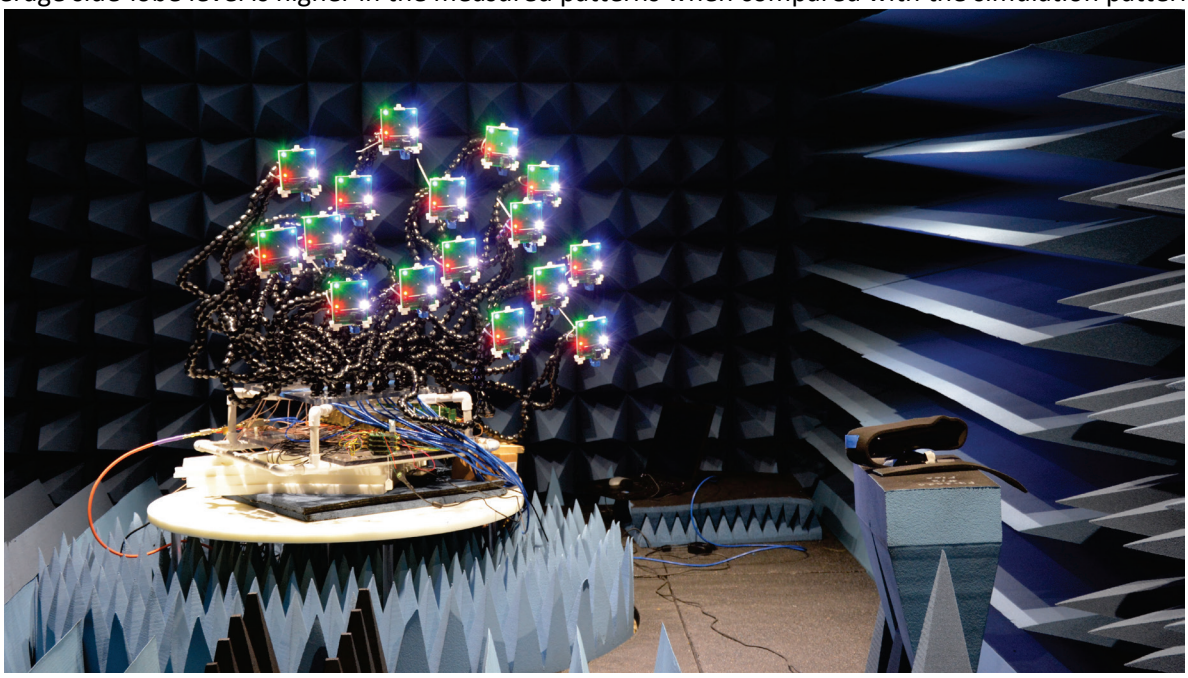

Fig. 40 The 16-element test apparatus with movable elements (named Medusa).

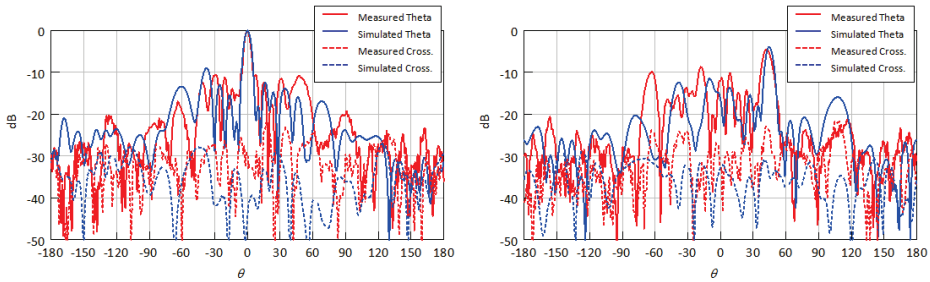

Fig. 41 (Left) ($\vartheta=0,\phi=0$) Measured and simulated normalized broadside pattern (Right) ($\vartheta=45,\phi=0$) measured and simulated normalized Theta radiation pattern.

This computer vision assisted framework for beamforming and geolocation of swarming antenna arrays represents a major accomplishment of this project, and the accumulation of nearly every performance period in this program. This was engineered to both study and interact with phased arrays formed by randomly distributed clusters of antennas (e.g., swarms), and it provides a viable tool to study and control the radiation behavior and other characteristics of volumetric, planar, and other distributions as elements move and the topology of the cluster morphs. Complex control, element identification, and beam steering have been experimentally demonstrated for a number of test cases. Simulation and measured results for basic beam steering scenarios illustrated the overall effectiveness and utility of the system. The system was also used to track morphing clusters and swarms of elements, and the system presents an opportunity for further investigation into radiation characteristics of morphing swarms and how complex geometries in dynamic choreographed movements can be controlled to achieve desired radiation behavior.

Thrust 4 Other synergistic activities related to multifunctional antennas

Research Goal 4.1 Integrating reconfigurable antennas into software-defined radio architectures
PI: Gregory H. Huff
PhD Graduate Student: Jeffrey S. Jensen
Undergraduate Student: Thomas Matthews

This senior design project utilized software defined radios for the development of a cognitive radio system. A polarization reconfigurable crossed dipole antenna using high-speed photodiodes was designed, fabricated, and connected to a variable-gain amplifier – each were controlled by a microcontroller which was connected to and controlled by a transmit-receive pair of commercially available universal software-defined radio platforms (USRP) operating in the ISM band. A program in C++ was written for the FPGA on the USRP which monitored the bit error rate (BER) and switched antenna configurations (polarization) similar to a switched diversity system, and adjusted the gain of the amplifier if a suitable channel could not be found. Several other projects related to dynamic networks and smart phone applications are underway. This includes using the smart phone to control complex RF systems. An ongoing collaboration between the PI and faculty in the Wireless Communications Group is facilitating this work on multifunctional wireless platforms to enhance complex content distribution and increase coverage in electromagnetically hostile environments.

Research Goal 4.2 Integrating reconfigurable antennas into software-defined radio architectures
PI: Gregory H. Huff
PhD Graduate Student: Jeffery S. Jensen
PhD Graduate Student: Kristopher Buchannan
MS Graduate Student: Taahir Ahmed

This project examined the performance of remotely located clusters of wireless communication nodes, and portable on-the-move swarming technologies that have the potential to provide a range of unique enabling capabilities when deployed in a network-centric topology. Using the swarm geometric structure for collaborative beamforming, the enrichment of basic communications, as well as, enhance security through superior resolution characteristics, was studied where the cluster of radiators can exploit the spatial setting of available resources in a distributed beamforming framework. The topology of the cluster and distribution of elements were fund to be key parameters to consider when evaluating the performance capabilities of aperiodic arrangements for stationary, quasi-stationary, or even mobile configurations. Furthermore, because the physical mechanisms describing the beamforming process are complicated enough that relying on a complete description of the pattern can become impractical, an estimation of beamforming performance based on a geolocation-derived expected beam patterns was shown to be adequate in a number of scenarios.

Research Goal 4.3 *Multifunctional coatings and energy harvesting concepts for deployment of UGS*
Integrating reconfigurable antennas into software-defined radio architectures
PI: Gregory H. Huff
PhD Graduate Student: David Rolando

Multifunctional coatings have been integrated into the design of the SIFA and a preliminary study into the stability of its electromagnetic performance was performed. This assumed i8t was dropped with a random orientation onto a lossy earth-like material. Such SIFAs could be deployed into a remote environment for telemetric, communication, or other collaborative purposes. Each SIFA would thus

serve as a single node in sparse and aperiodic-populated ad-hoc network that could potentially add phased array or digital beamforming capabilities (providing synchronization can be achieved). The notional simulation scenario (shown inFig. 42) was devised to test the SIFA's deployed performance in a two-node communication link. Two SIFAs (one a transmitter Tx, the other a receiver Rx) are placed above (nearly touching) a lossy dielectric ground in this scenario; the ground is assumed to be flat so that a line-of-sight (LOS) link exists between the antennas (multipath was also examined). Both antennas were assumed to be randomly oriented above the ground and rotated around two axes to a specific position. This provided a first step in analyzing remote operation for the SIFA.

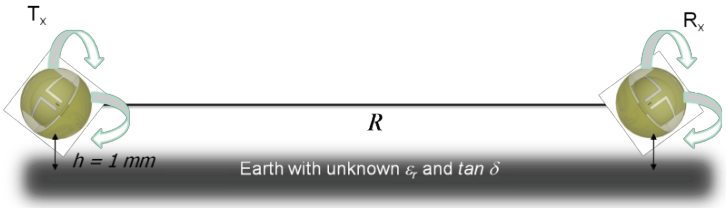

Fig. 42 Simulation scenario for two randomly orientated SIFAs located above a lossy earth material.

It is of significant interest to compare the performance of the original uncoated SIFA design to a coated design in the two node link scenario described above. The coated design promises many possible advantages. A durable coating can provide a physical advantage of protection for the antenna from harsh environmental conditions as well as structural rigidity and a coating can provide electromagnetic advantages. It can also provide electromagnetic advantages if the coating is made out of a high dielectric material; this will minimize the adverse effects of being in the presence of unknown dielectric surroundings to improve the predictability of the antennas' of performance (e.g., the antennas will remain more stable at the desired operating frequency). Fig. 43 shows a fabricated SIFA with a carbon-microfiber reinforced silicone rubber coating; this structure was used in simulations after scaling its size to account for dielectric loading. Fig. 43 also shows the normalized probability distribution function (PDF) of the VSWR and received power (for a nominal input power and far-field separation) for a full range of rotations and orientations. These curves show the stabilizing effect of the coating and the impact of both lossy materials and antenna miniaturization on the received power. Antenna miniaturization creates the most significant impact in power received power due to the physical limitations based on the antennas radiation efficiency (e.g., its ability to couple energy into a free-space wavelength).

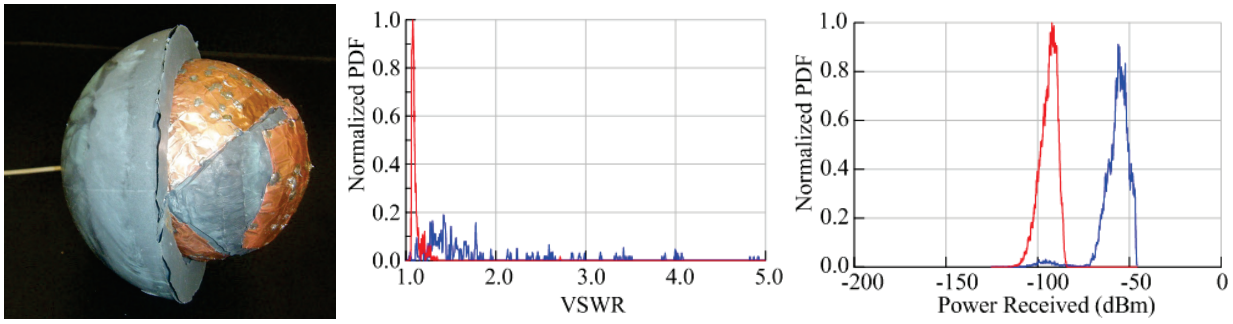

Fig. 43 Fabricated SIFA with a latex rubber and carbon-black composite coating (left); normalized probability distribution function (PDF) of the VSWR and received power (for a nominal input power and far-field separation) for a full range of rotations and orientations for the uncoated (middle) and coated (left) SIFAs.

Research Goal 4.4 Direction of arrival techniques integrating the MUSIC algorithm with Extended Kalman Filters and dual-band networks, and implementing the hybrid algorithm for small volumetric arrays with random, periodic, and crystallographic-based lattices
PI: *Gregory H. Huff*
PhD Graduate Student: *Zhenchun Xia*

Analytical and experimental work related to direction of arrival was performed in this project. The analytical work pertains to an integrated algorithm that includes a Kalman filter for tracking and stabilization, Kent distributions for estimation of statistical directional information, wide-band antennas and polarization-reconfigurable antennas for spatial and frequency diversity, sparse arrays for anti-aliasing, and a real-time measurement set-up for estimation of DOA information. An experimental system used to test these algorithms has been constructed using an 18-way electromechanical switching network and transmitter antenna that are connected to the PNA and controlled using LabView, a DAQ, and peripheral circuitry. This switched network was be capable of measuring the phase difference between the antennas for DOA estimation and algorithm testing. Fig. 44 shows the real-time testing system constructed at National Instruments' facility in Austin, TX. This is connected to a disjointed array of vertical and horizontal linear arrays in crystallographic configurations (tetragonal and cubic).

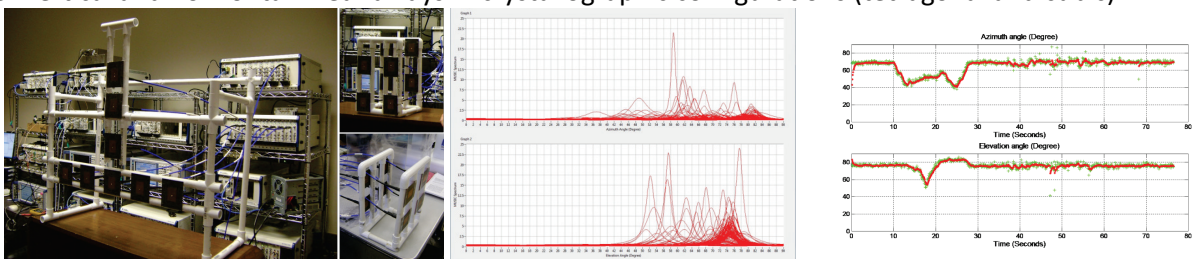

Fig. 44 Real-time testing system constructed at National Instruments with a planar array and two of the volumetric arrays (left), snapshots of the calculated MUSIC spectrum at different instants in time while the transmitter is moving (middle), and real time estimation of DOA with moving transmitter (Green curve: without additional signal processing; Red curve: with additional signal processing) (right).

The results for a static (fixed) angle of incidence were measured and computed first so the performance of the real-time acquisition system and algorithm could be verified. Measured and simulated results showed good agreement to analytical expectations. The system was then used to examine a tracking capabilities and real-time performance using a sampling rate of the eight-channel system of 10 Hz. A series of these measurements with a moving transmitter have been overlaid in Fig. 44 at different snapshots in time. When these results are translated into the plot of DOA vs. time (right side of Fig. 44) the real-time tracking of the DOA's azimuthal and elevation can be seen (green dots). With some additional signal processing, the performance can be improved (red line).

Research Goal 4.2 Multifunctional buoy-based Antensors for disturbance localization and monitoring
PI: *Gregory H. Huff*
PhD Graduate Student: *David Rolando*
PhD Graduate Student: Narayanan Rengaswamy
Undergraduate Student: *Alyssa Bennet*
Undergraduate Student: *Jake McKnight*

This undergraduate research project focused on integrating an inertial measurement unit (IMU), an ISM 900 MHz transceiver, and a GPS receiver into the unused and shielded volumetric regions of the spherical inverted F-antenna. The antenna was 3D printed and metalized accordingly, and Fig. 45 Fig. 20 shows the current application framework developed in Qt which reads in the IMU data from the

antenna-buoy (multifunctional antenna) and performs all of the calculations in real time. This application incorporates GPS and IMU data in a modified MUSIC algorithm. The algorithm exploits the non-linear wave propagation of shallow water waves to create a unique set of basis functions for the algorithm, and then examines the intersection of time-of-arrival solutions (circles) to establish the location of a water disturbance.

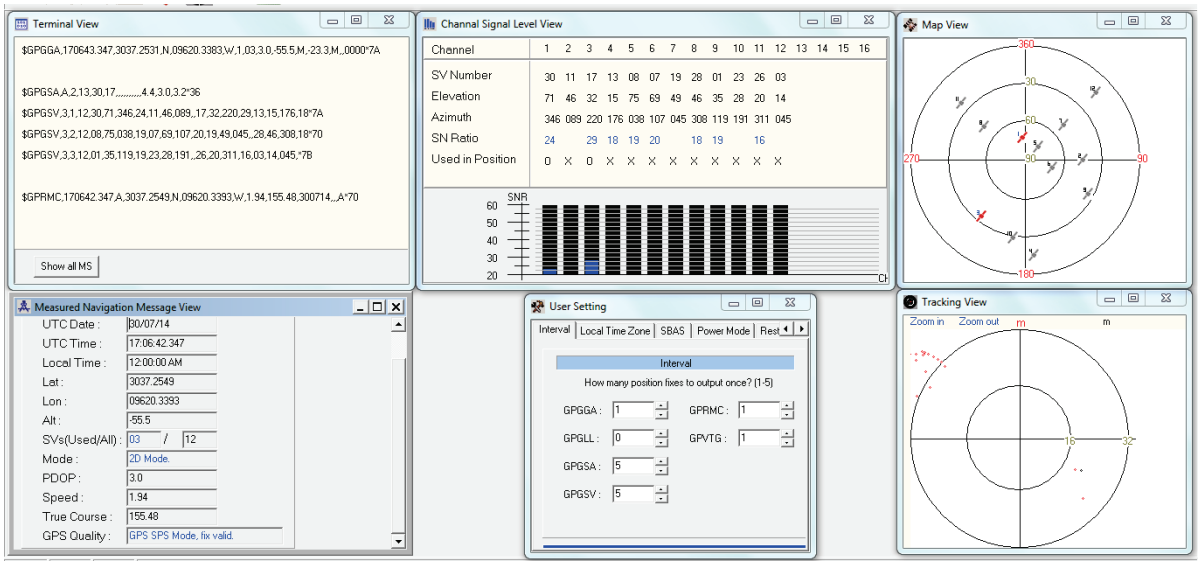

Fig. 45 Application framework developed in Qt which reads in the IMU data from the antenna-buoy network (multifunctional antennas) and calculated the disturbance in the water.

Fig. 46 shows several views of the SIFA that was modified as a water-tight sensor module for deployment as an oceanographic monitoring tool (multifunctional antenna). It was made from copper tape that is mounted onto a quarter hemisphere substrate made of ABS plastic (using the 3D printer). This shell functions to protect the SIFA from the elements. The measured and simulated (HFSS) impedance and VSWR are provided in Fig. 47.

Fig. 46. Substrate and antenna of SIFA (upper left), top hemisphere and substrate (upper right), SIFA sitting next to bottom hemisphere with charging port located in center of bottom hemisphere (lower left), and perspective view of the SIFA mounted on the bottom hemisphere (outer shell not shown) (bottom right).

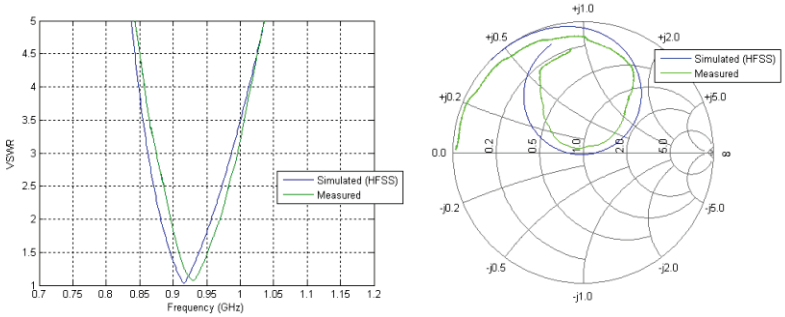

Fig. 47. Measured and simulated (HFSS) impedance and VSWR of the module shown in Fig. 46.

Each antenna-buoy was outfitted with a sensor package that was located inside the SIFA to capture motion data and isolate it from the water. Each data node sends a data packet labeled with the node's identity and each sensor's identity in response to the center node's request. The center node connects to a computer. The laptop computer receives the data from the star network from the central node via its serial port and the data read from the serial port is sent to a MySQL database. In this configuration the SIFA acts as a buoy which is buoyant and sits atop the water line and collects IMU data on the motion of waves. The open-source MATLAB program "Shallow Water Waves" was used to model a disturbance in water generating shallow-water gravity waves. Data from the waveform generated from the disturbance was collected from various known locations during the simulation and logged into a matrix, referred to as the master matrix. These formed the set of basis (test) functions for the MUSIC algorithm, which are used to estimate the time of arrival of the wave by comparing its recorded motion to the analytically-derived value. Then, using the recorded time-normalized wave profiles for locations along a radial direction, the disturbance can be triangulated.

Research Goal 4.3 A modular framework for using reconfigurable antenna arrays in an autonomous direction of arrival estimation system
PI: *Gregory H. Huff*
Undergraduate Student:*E. S. Foster*
Undergraduate Student: *R. D. Haley*
Undergraduate Student: *Q. E. Manley*
Undergraduate Student: *R. D. Moore*

An Android smartphone-controlled direction of arrival system was developed which uses independently-controllable polarization-reconfigurable antennas. A modular framework was also deployed using a remote (cloud-based) data acquisition and processing server scheme. An Android smartphone application (app) provides the user interface for the system and can be used to select the polarization state of each of the antennas in the array as well as view/monitor data as it is made available at the server. Two servers function to coordinate the acquisition process, gather measurement data, process the received phase information to generate direction of arrival information using the MUSIC algorithm, and provide other remote system monitoring functions. The diagram and fabricated system are shown in Fig. 48, and the polarization-reconfigurable antenna design is provided in Fig. 49.

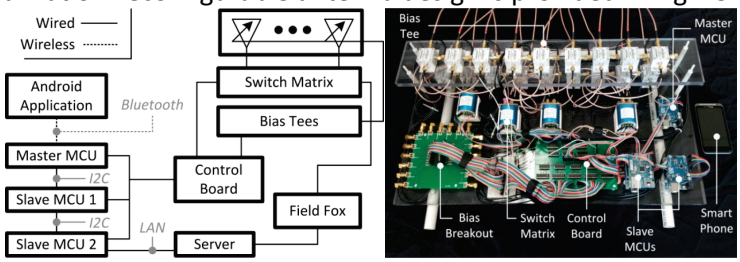

Fig. 48 (Left) Basic layout of modules and the types of communication scheme used to pass data and control between them and (right) fully-assembled antenna array controller.

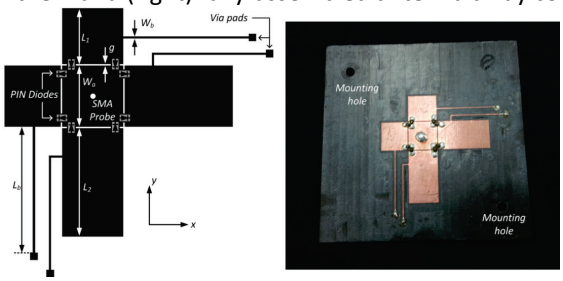

Fig. 49 (Left) Diagram and (right) fabricated polarization-reconfigurable antenna.

The reconfigurable antenna was designed to facilitate two reconfigurable polarization states. The design consists of two identical narrow patch antennas that are orthogonally-overlaid about the SMA probe feed location. Quarter-wave high impedance short-circuit bias lines terminated in connect each arm to DC and RF ground and two RF PIN diodes are placed across each of the gaps such that the central patch region has in a common-cathode and common-anode connection in the x- and y-directions, respectively. In this configuration (where the antenna's ground plane doubles as the DC ground) a single control voltage delivered can be delivered through the probe feed using a coaxially-connected bias-tee to apply a positive or negative voltage to switch between the x- and y-aligned narrow patches. Hence, a positive bias voltage applied to the central patch region forward-biases the diodes on that arm and polarizes the antenna in according to the *x-dir.* patch. A negative bias voltage turns on the previously reverse-biased diodes and polarizes the antenna according to the *y-dir.* patch. These were placed in circular, random, and linear array configurations (Fig. 50) and measurements were performed using the remote acquisition and processing system. The measured results were in agreement with expectations; results for the random array with the beacon positioned 30° to the right of the array are shown in Fig. 51. The MUSIC spectrum generated from the measured and simulated data show aliasing 30° from the -180° position because arrays are planar arrays and therefore cannot resolve the difference between a signal incident from the front and back of the array (aliasing). The results generated using the circular array contains more structured noise than the results generated using the random array due to the circular array's periodic spacing.

Fig. 50 Circular, random, and linear array configurations.

Fig. 51 Normalized music spectrum of the random array generated using simulated (left) and measured (right) data from the autonomous data collection system.

Technology Transfer

There is no activity to report on technology transfer.